inetics and topical application of drugs. In Fitzpatrick's Dermatology in General Medicine (Freedberg, I., Eisen, A., Wolff, K., Austen, F., Goldsmith, L. and Katz, S. eds.), pp.2313-2318, McGraw-Hill, New York.

Senzui, M., Tamura, T., Miura, K., Ikarashi, Y., Watanabe, Y. and Fujii, M. (2010): Study on penetration of titanium dioxide (TiO(2)) nanoparticles into intact and damaged skin in vitro. J. Toxicol. Sci., **35**, 107-113.

Suzuki, M. (1987): Protective effect of fine-particle titanium dioxide on UVB-induced DNA damage in hairless mouse skin. Photodermatol., **4**, 209-211.

Wu, J., Liu, W., Xue, C., Zhou, S., Lan, F., Bi, L., Xu, H., Yang, X. and Zeng, F.D. (2009): Toxicity and penetration of TiO2 nanoparticles in hairless mice and porcine skin after subchronic dermal exposure. Toxicol. Lett., **191**, 1-8.

Xu, J., Sagawa, Y., Futakuchi, M., Fukamachi, K., Alexander, D.B., Furukawa, F., Ikarashi, Y., Uchino, T., Nishimura, T., Morita, A., Suzui, M. and Tsuda, H. (2011): Lack of promoting effect of titanium dioxide particles on ultraviolet B-initiated skin carcinogenesis in rats. Food Chem. Toxicol., **49**, 1298-1302.

Xu, J., Futakuchi, M., Iigo, M., Fukamachi, K., Alexander, DB., Shimizu, H., Sakai, Y., Tamano, S., Furukawa, F., Uchino, T., Tokunaga, H., Nishimura, T., Hirose, A., Kanno, J. and Tsuda, H. (2010): Involvement of macrophage inflammatory protein 1alpha (MIP1alpha) in promotion of rat lung and mammary carcinogenic activity of nanoscale titanium dioxide particles administered by intra-pulmonary spraying. Carcinogenesis, **31**, 927-935.

Cancer Science
The official journal of the Japanese Cancer Association

Dose-dependent mesothelioma induction by intraperitoneal administration of multi-wall carbon nanotubes in p53 heterozygous mice

Atsuya Takagi,[1] Akihiko Hirose,[2] Mitsuru Futakuchi,[3] Hiroyuki Tsuda[4] and Jun Kanno[1,5]

[1]Division of Cellular and Molecular Toxicology, [2]Division of Risk Assessment, Biological Safety Research Center, National Institute of Health Sciences, Tokyo; [3]Department of Molecular Toxicology, Nagoya City University Graduate School of Medical Sciences; [4]Nanomaterial Toxicology Project Laboratory, Nagoya City University, Nagoya, Japan

(Received February 21, 2012/Revised March 25, 2012/Accepted April 22, 2012/Accepted manuscript online April 27, 2012/Article first published online June 21, 2012)

Among various types of multi-wall carbon nanotubes (MWCNT) are those containing fibrous particles longer than 5 μm with an aspect ratio of more than three (i.e. dimensions similar to mesotheliomagenic asbestos). A previous study showed that micrometer-sized MWCNT (μm-MWCNT) administered intraperitoneally at a dose of 3000 μg/mouse corresponding to 1×10^9 fibers per mouse induced mesotheliomas in p53 heterozygous mice. Here, we report a dose-response study; three groups of p53 heterozygous mice ($n = 20$) were given a single intraperitoneal injection of 300 μg/mouse of μm-MWCNT (corresponding to 1×10^8 fibers), 30 μg/mouse (1×10^7) or 3 μg/mouse (1×10^6), respectively, and observed for up to 1 year. The cumulative incidence of mesotheliomas was 19/20, 17/20 and 5/20, respectively. The severity of peritoneal adhesion and granuloma formation were dose-dependent and minimal in the lowest dose group. However, the time of tumor onset was apparently independent of the dose. All mice in the lowest dose group that survived until the terminal kill had microscopic atypical mesothelial hyperplasia considered as a precursor lesion of mesothelioma. Right beneath was a mononuclear cell accumulation consisting of CD45- or CD3-positive lymphocytes and CD45/CD3-negative F4/80 faintly positive macrophages; some of the macrophages contained singular MWCNT in their cytoplasm. The lesions were devoid of epithelioid cell granuloma and fibrosis. These findings were in favor of the widely proposed mode of action of fiber carcinogenesis, that is, frustrated phagocytosis where the mesotheliomagenic microenvironment on the peritoneal surface is neither qualitatively altered by the density of the fibers per area nor by the formation of granulomas against agglomerates. (*Cancer Sci* 2012; 103: 1440–1444)

Unique properties such as persistency and electric conductivity promise a high potential for technology applications of carbon nanotubes (e.g. in lithium ion batteries). Immediately after the invention of the carbon nanotube, its persistency and fibrous shape have posed a challenge for toxicology known as "fiber carcinogenesis".[1] A recent study showed that a particular type of multi-wall carbon nanotube (Mitsui MWCNT-7, designated in general here as micrometer-sized MWCNT or μm-MWCNT) contains a considerable percentage of particles similar to asbestos in length and diameter.[2] To investigate its mesotheliomagenic potential, we used an intraperitoneal injection (i.p.) method that was extensively used in the 1970s and 1980s for the elucidation of key dimensions of the fiber (e.g. length and diameter) and for toxicity assessment of various man-made fibers.[3–6] Although the route of exposure is not realistic for humans, the i.p. injection method has been considered appropriate to assess the mesotheliomagenic potential of fibers,[7] and the least potent fibers were found to induce a positive result at a dose of 10^9 fibers i.p. in rats.[6–8]

Our first study identified the mesotheliomagenic potency of Mitsui MWCNT-7 at a single maximum dose (i.e. 10^9 fibers) in the peritoneal cavity of p53 heterozygous (p53+/−) mice[2] (data shown as a reference in Fig. 1). Marsella *et al.*[9] has shown that development of mesothelioma by crocidolite asbestos was accelerated in this mutant mouse. We have bred this mouse and tested it as an alternative model to replace the wild-type mouse carcinogenicity test of the National Toxicology Program of the National Institute of Environmental Health Sciences/NIH of the United States.[10] As a result, spontaneous neoplastic lesions of this model have been well characterized.[11]

Here, we applied the same fiber to p53+/− mice at doses of 1/10, 1/100, and 1/1000 of the dose used in the previous study (i.e. 300, 30 and 3 μg/mouse), which corresponds to approximately 1×10^8, 1×10^7, and 1×10^6 fibers per mouse, respectively, and monitored the mice for 1 year.

Materials and Methods

Experimental animals. The p53+/− mice were generously supplied by Dr S. Aizawa,[12] and back crossed with normal wild-type C57BL/6 females (SLC, Shizuoka, Japan) for more than 20 generations at the National Institute of Health Sciences (NIHS), Tokyo. Eighty male p53+/− mice aged 9–11 weeks were divided into four groups of 20 mice, and housed individually under specific pathogen-free conditions with a 12-h light-dark cycle at a NIHS animal facility. They were given tap water and autoclaved CRF-1 pellets (Oriental Yeast Co. Ltd., Tokyo, Japan) *ad libitum*. Experiments were humanely conducted under the regulation and permission of the Animal Care and Use Committee of the NIHS.

Histology. Liver, kidney, spleen, lung, digestive tract and macroscopic tumors (*en bloc* in the case of severe peritoneal adhesion) were fixed in 10% neutral buffered formalin. After conventional processing, paraffin-embedded sections were stained with hematoxylin–eosin (HE) and examined histopathologically under a light microscope. A pair of polarizing filters was set to a light microscope to detect birefringent particles.

For the selected atypical mesothelial hyperplasia lesions, serial sections were stained for CD45R(B220), CD3 and F4/80 using anti-mouse CD45R (eBioscience, San Diego, CA, USA), anti-rat CD3 (AbD Serotec, Kidlington, UK), anti-mouse F4/80 antibodies (eBioscience), which were diluted at 1:100, 1:50 and 1:50, respectively. The slides were incubated at 4°C overnight

[5]To whom correspondence should be addressed.
E-mail: kanno@nihs.go.jp

doi: 10.1111/j.1349-7006.2012.02318.x

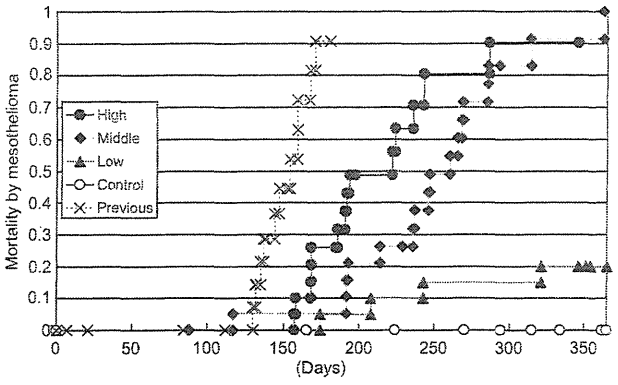

Fig. 1. Dose-dependent induction of mesotheliomas by micrometer-sized multi-wall carbon nanotubes (μm-MWCNT). Mice with lethal mesotheliomas are plotted using the Kaplan–Meier method. High: 300 μg/mouse, corresponding to 1×10^8 fibers/mouse; middle: 30 μg/mouse, corresponding to 1×10^7 fibers/mouse; low: 3 μg/mouse, corresponding to 1×10^6 fibers/mouse); previous: data from a previous study (i.e. 3 mg/mouse, corresponding to 1×10^9 fibers/mouse). No mesothelioma was observed in the vehicle control group.

and then incubated for 1 h with biotinylated species-specific secondary antibodies diluted 1:500 (Vector Laboratories, Burlingame, CA, USA) and visualized using avidin-conjugated alkaline phosphatase complex (ABC kit; Vector Laboratories).

Test material. Multi-wall carbon nanotube (MITSUI MWCNT-7, Lot No. 060125-01k), the same lot used in our previous study[2] was used. As reported in our previous paper, one gram of MWCNT corresponded to 3.55×10^{11} particles. The length ranged from 1 to 20 μm with a median of 2 μm. More than 25% of the particles were longer than 5 μm; their width ranged from 70 to 170 nm with a median of 90 nm. The approximate average content of iron was 3500 ppm (0.35%) and that of sulfur was 470 ppm. The concentration of chlorine in the fibers was 20 ppm and that of fluorine and bromine was below the limits of detection (5 and 40 ppm, respectively).[2]

Multi-wall carbon nanotubes was suspended at a concentration of 3 mg/mL to 0.5% methyl cellulose (Shin-Etsu Chemical Co. Ltd, Tokyo, Japan) solution and autoclaved (121°C, 15 min). After addition of Tween 80 (Tokyo Chemical Industry Co. Ltd, Tokyo, Japan; final 1.0% concentration), the solution was subjected to sonication at 150 watt for 5 min using an ultrasonic homogenizer (VP30s; TAITEC Co., Saitama, Japan).

Treatment. Eighty male p53+/− mice aged 9–11 weeks were randomly divided into four groups of 20. The high-dose group mice were given a single i.p. injection of 300 μg/mouse of MWCNT particles (corresponding to 1×10^8 fibers) in 1 mL suspension. The middle-dose group mice received 30 μg/mouse (1×10^7) and the low-dose group mice received 3 μg/mouse (1×10^6), respectively. The control group mice received vehicle solution (1 mL). Treated mice were monitored for 1 year. To minimize stress to the animals and re-aggregation of suspension, the injection was promptly performed without anesthesia.

Results

Peritoneal mesotheliomas were induced in a dose-dependent manner shown by an increase in the cumulative incidence of the tumors (Fig. 1). In the high-dose group, 14/20 mice had single or multiple lethal mesotheliomas up to 2 × 2 cm in size located within the peritoneal cavity, invading adjacent organs and structures with or without peritoneal dissemination. The remaining mice died of ileus due to severe peritoneal adhesion and fibrosis, and among them five had small incidental (non-lethal) mesotheliomas. The total incidence of mesothelioma was 19/20 (95%) among the animals. These lesions were qualitatively identical to our previous study.[2] In the middle-dose group, 17/20 (85%) mice had lethal mesothelioma. Three mice without lethal mesothelioma died or became moribund due to other reasons including leukemia. In the low-dose group, 4/20 mice had lethal mesothelioma (Fig. 2) and 1/20 had a non-lethal mesothelioma (found at the terminal kill on day 365), which makes the overall incidence of mesothelioma 5/20 (25%). The other 15 mice that survived until the terminal kill showed focal mesothelial atypical hyperplasia.[13] These lesions, up to 0.5 mm in diameter, consisted of a single layer of mesothelium characterized by cuboidal or hobnail appearance with slight to moderate nuclear atypia. Right beneath the

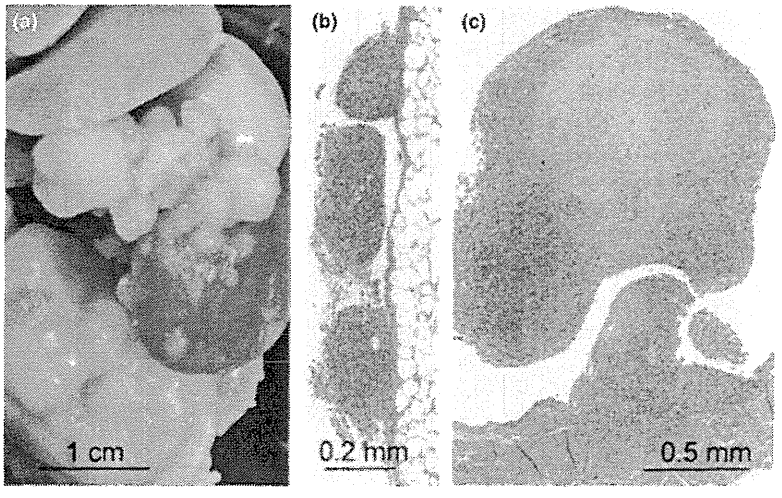

Fig. 2. Morphology of the induced mesotheliomas in the low-dose group. (a) Macroscopic view of the abdominal cavity of a mouse in the low-dose group. Multiple nodules are seen on the surface of the peritoneal serosa. This mouse died on day 243 with multiple nodules up to size 1 × 1 × 1 cm. (b) Low-power light microscopy view of the multiple nodules on the peritoneal surface of the mesentery. Granulomas and fibrous scars are minimal in the low-dose group. (c) Histology of a small nodule compatible with a diagnosis of moderately to poorly differentiated epithelioid mesothelioma. Larger nodules tended to be composed of undifferentiated sarcomatous components.[2]

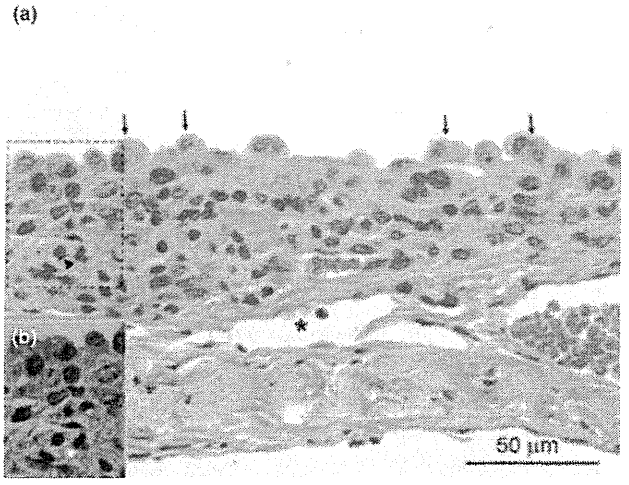

Fig. 3. Atypical mesothelial hyperplasia. (a) Atypical mesothelial hyperplasia of the tendinous portion of the diaphragm of a mouse in the low-dose group (sampled at terminal kill, that is, 365 days after i. p. inoculation of the multi-wall carbon nanotubes [MWCNT]). Arrows: hobnail appearance of the atypical hyperplastic mesothelial cells; asterisk: lymphatic drainage of the peritoneal cavity. (b) Polarized image of the dotted area in (a). Arrowhead: a MWCNT fiber in a macrophage-like cell (birefringent).

atypical mesothelium was a lentiform accumulation of mononuclear inflammatory cells up to 0.1 mm in thickness (Fig. 3). The accumulation is a combination of ill-demarcated zones of CD45-positive lymphocytes, CD3-positive lymphocytes and CD45/CD3-negative F4/80-negative or CD45/CD3-negative F4/80 weakly positive macrophage-like cells (Fig. 4). Single MWCNT fiber was often found in the cytoplasm of the macrophage-like cells. These lesions were devoid of epithelioid cell granuloma and fibrous scars.

Peritoneal fibrosis, peritoneal adhesion and formation of foreign body granulomas towards agglomerated MWCNT were dose dependent and minimal in the low-dose group. In the control group, mesotheliomas were not found (0%). There were eight mice with lethal or incidental thymic lymphoma, leukemia or reticulum cell sarcoma, osteosarcoma of the cranial bone, and 12/20 were tumor free. These tumors are known to develop spontaneously in p53+/− mice with increasing age[10] and none of these tumors were treatment dependent.

Histology of the mesotheliomas ranged from a differentiated epithelioid type to an undifferentiated sarcomatous type. Osteoid and rhabdoid differentiations, both known in human cases,[14–16] were found in nine mice (two in the low dose, three in the middle dose, and four in the high dose group, respectively) among a total of 41 mesothelioma cases in the present study.

An additional finding was the dissemination of singular fibers to systemic organs such as the liver, mesenteric lymph nodes, pulmohilar lymph nodes, choroid plexus of the brain, glomeruli of the kidney and lung alveoli (Fig. 5). Because the brain, including the choroid plexus, lacks afferent lymphatics,[17,18] it is probable that the fibers were distributed systemically via the blood stream.

Discussion

The present study showed a dose-dependent induction of mesothelioma by the μm-MWCNT from 1/1000 of the dose of our previous study (i.e. 3 μg/mouse corresponding to 1×10^6 fibers).

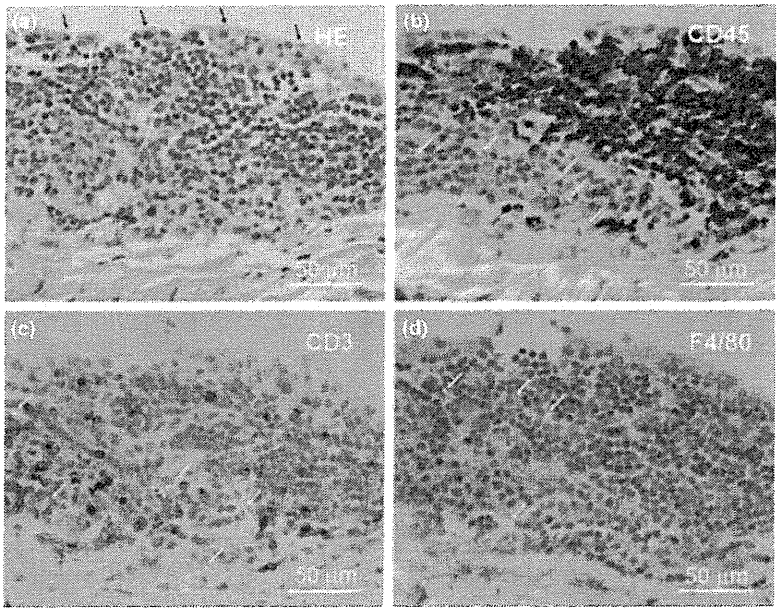

Fig. 4. Immunohistochemistry of lentiform mononuclear cell accumulation underlying the atypical mesothelial hyperplasia. (a) Serial section of an atypical mesothelial hyperplasia of the tendinous portion of the diaphragm of a mouse in the low-dose group (sampled at terminal kill). (a) Hematoxylin–eosin staining. Black arrows: hobnail appearance of the hyperplastic mesothelial cells. (b–d) Polarized image of the serial sections immunohistochemically stained for CD45, CD3 and F4/80. Multi-wall carbon nanotubes (birefringent; white arrows) are seen in the macrophage-like CD45/CD3-negative, F4/80-faintly positive cell cytoplasm. It is noted that epithelioid cell granuloma and fibrous scars are absent in this type of lesion.

doi: 10.1111/j.1349-7006.2012.02318.x

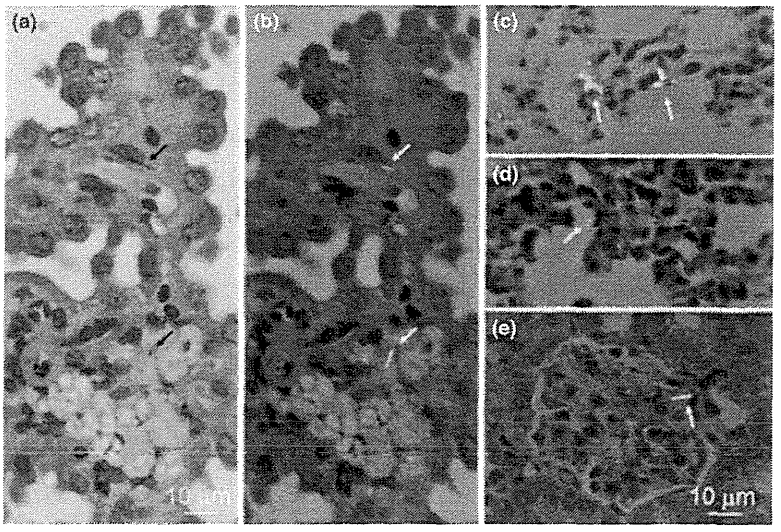

Fig. 5. Systemic distribution of singular fibers. Single micrometer-sized multi-wall carbon nanotube fibers are found in the choroid plexus in (a) normal lighting and (b) polarized light (in a mouse from the high-dose group sampled on day 168), (c) lung as an agglomerate within macrophages (polarized light) or (d) as singular fibers (polarized light) and (e) a renal glomerulus (polarized light) (in a mouse from the high-dose group sampled on day 197). Fibers were also found in hepatic sinusoids and mesenteric lymph nodes (not shown).

It is noted that the mesotheliomas of the low-dose group were not accompanied by foreign body granulomas or fibrous scars. The mesothelial atypical hyperplasia found 1 year after the i.p. injection in the low-dose group mice were also devoid of foreign body granulomas and fibrous scars. Instead, these lesions were backed up by an accumulation of mononuclear inflammatory cells. The macrophage-like cells in the accumulation, negative to weakly positive for F8/40, were often positive for singular MWCNT in their cytoplasm. As the mesothelial atypical hyperplasia is considered as precancerous lesions, the essential background of mesotheliomagenesis might be the inflammatory lesions without granulomas and fibrous scars formed against MWCNT agglomerates. The mesothelial atypical hyperplasia can be regarded as a lesion driven by the frustrated phagocytosis against MWCNT.

In general, carcinogenesis is considered a multistage process. In the case of chemical carcinogens with clear genotoxic properties, tumor onset occurs significantly earlier at higher doses.[19,20] Presumably, an increasing number of hits to a target cell leads to faster progression of the carcinogenic stages. Here, in contrast, the onset time of the mesotheliomas was apparently dose independent. Onset estimates calculated as x-intercepts of logarithmic approximation[21,22] were 126, 146, 148 and 138 days for the previous study data[2] and the three doses of the present study, respectively (Fig. S1). Mechanistically, a direct effect to a mesothelial cell, such as mutagenic or clastogenic effect, would favor a dose-dependent acceleration of the onset. If the granulomas are an important promoting factor of mesotheliomagenesis,[23] the highest dose group should have had the earliest onset because the granuloma formation can take place within 7 days subsequent to the i.p. injection.[24] In contrast, the humoral stimuli released from the nearby macrophages in the condition of frustrated phagocytosis[25] would match with this finding. As shown in Figures 3 and 4, the reactive mesothelial cells are accompanied by mononuclear inflammatory cells with MWCNT fibers, but not by epithelioid cell granulomas or fibrous scars. One could speculate that each loci of frustrated phagocytosis could continuously stimulate the nearby mesothelial cells, that is, first to induce reactive hyperplasia and then as the next step proceed towards mesothelioma. If the dose is the determinant of the number of such loci within a defined surface area of peritoneal mesothelial membrane, then it is natural to predict that the earliest day of tumor onset is dose independent, whereas the probability of tumor onset closer to the earliest day will increase in a dose-dependent manner.

An additional finding was the distribution of singular fibers to systemic organs such as the liver, mesenteric lymph nodes, pulmohilar lymph nodes, choroid plexus of the brain, glomeruli of the kidney and lung alveoli (Fig. 5). Because the brain, including the choroid plexus, lacks afferent lymphatics,[17,18] it is probable that the fibers were distributed systemically via the blood stream. Its importance to human health could be closely linked to the systemic distribution of asbestos reported in humans,[26,27] that is, a possibility of increasing systemic diseases such as cancer in various organs[28] and autoimmune diseases.[29] *In vivo* studies on the shorter fractions of MWCNT for its systemic toxicity would be essential.

It is likely that the peritoneal cavity served as a filter to segregate large agglomerates from the i.p. injected MWCNT suspension by the formation of foreign body granulomas and fibrous scars, leaving singular long MWCNT fibers for mesotheliomagenesis (frustrated phagocytosis) and short singular fibers for systemic distribution. The short fibers might have passed through the stomata (pores) of the mesothelium[23] or been transported by macrophages into lymphatics and to the vascular systems. As a whole, the i.p. injection model appears to be a robust system for the hazard identification of fiber carcinogenesis of asbestos-like fibrous particulate matter and of systemic toxicity of fibrous and non-fibrous particulate matter including nanoparticles that can enter the blood stream.

In conclusion, μm-MWCNT was mesotheliomagenic in the p53+/− mouse peritoneal cavity model in a dose-dependent manner from as low as 3 μg per mouse or approximately 10^6 fibers per mouse. Although the molecular mechanisms of fiber mesotheliomagenesis are unknown, the minute lesions seen in the lowest dose group and the dose-response characteristics might be consistent with the concept of frustrated phagocytosis and also with the observation in human asbestos epidemiology

that there would be no practical threshold for fiber mesotheliomagenesis.

Acknowledgments

The authors thank Mr Masaki Tsuji for technical support, and Dr Robert R. Maronpot and Dr Kai Savolainen for critical reading of the manuscript. The present study was supported by Health Sciences Research Grants H18-kagaku-ippan-007 and H21-kagaku-ippan-008 from the Ministry of Health, Labour and Welfare, Japan.

Disclosure Statement

The authors have no conflict of interest.

References

1 Service RF. CHEMISTRY: nanotubes: the next asbestos? *Science* 1998; **281**: 941.
2 Takagi A, Hirose A, Nishimura T *et al.* Induction of mesothelioma in p53+/− mouse by intraperitoneal application of multi-wall carbon nanotube. *J Toxicol Sci* 2008; **33**: 105–16.
3 Stanton MF, Layard M, Tegeris A *et al.* Relation of particle dimension to carcinogenicity in amphibole asbestoses and other fibrous minerals. *J Natl Cancer Inst* 1981; **67**: 965–75.
4 Pott F, Roller M, Kamino K, Bellmann B. Significance of durability of mineral fibers for their toxicity and carcinogenic potency in the abdominal cavity of rats in comparison with the low sensitivity of inhalation studies. *Environ Health Perspect* 1994; **102**(Suppl 5): 145–50.
5 Adachi S, Yoshida S, Kawamura K *et al.* Inductions of oxidative DNA damage and mesothelioma by crocidolite, with special reference to the presence of iron inside and outside of asbestos fiber. *Carcinogenesis* 1994; **15**: 753–8.
6 Roller M, Pott F, Kamino K, Althoff GH, Bellmann B. Dose-response relationship of fibrous dusts in intraperitoneal studies. *Environ Health Perspect* 1997; **105**(Suppl 5): 1253–6.
7 World Health Organization. *WHO Workshop on Mechanisms of Fibre Carcinogenesis and Assessment of Chrysotile Asbestos Substitutes*, 8–12 November 2005. Lyon, France: Summary Consensus Report World Health Organization, 2006.
8 European Chemicals Bureau. Carcinogenicity of synthetic mineral fibres after intraperitoneal injection in rats (ECB/TM/18(97) rev. 1). In: Bernstein DM, Riego Sintes JM. eds. *Methods for the Determination of the Hazardous Properties for Human Health of Man Made Mineral Fibres (MMMF) (EUR 18748 EN [1999])*. Ispra, Italy: Institute for Health and Consumer Protection, Unit: Toxicology and Chemical Substances, 1999; 41–52. [Cited 26 May 2012.] Available from URL: http://tsar.jrc.ec.europa.eu/documents/Testing-Methods/mmmfweb.pdf.
9 Marsella JM, Liu BL, Vaslet CA, Kane AB. Susceptibility of p53-deficient mice to induction of mesothelioma by crocidolite asbestos fibers. *Environ Health Perspect* 1997; **105**(Suppl 5): 1069–72.
10 Mahler JF, Flagler ND, Malarkey DE, Mann PC, Haseman JK, Eastin W. Spontaneous and chemically induced proliferative lesions in Tg.AC transgenic and p53-heterozygous mice. *Toxicol Pathol* 1998; **26**: 501–11.
11 Eastin WC, Haseman JK, Mahler JF, Bucher JR. The National Toxicology Program evaluation of genetically altered mice as predictive models for identifying carcinogens. *Toxicol Pathol* 1998; **26**: 461–73.
12 Tsukada T, Tomooka Y, Takai S *et al.* Enhanced proliferative potential in culture of cells from p53-deficient mice. *Oncogene* 1993; **8**: 3313–22.
13 Chung A, Cagle PT, Roggli VL, eds. *Tumors of the Serosal Membranes*. Washington, DC: American Registry of Pathology, 2006.
14 Chalabreysse L, Guillaud C, Tabib A, Loire R, Thivolet-Bejui F. Malignant mesothelioma with osteoblastic heterologous elements. *Ann Pathol* 2001; **21**: 428–30.
15 Matsukuma S, Aida S, Hata Y, Sugiura Y, Tamai S. Localized malignant peritoneal mesothelioma containing rhabdoid cells. *Pathol Int* 1996; **46**: 389–91.
16 Ordonez NG. Mesothelioma with rhabdoid features: an ultrastructural and immunohistochemical study of 10 cases. *Mod Pathol* 2006; **19**: 373–83.
17 Courtice FC, Simmonds WJ. The removal of protein from the subarachnoid space. *Aust J Exp Biol Med Sci* 1951; **29**: 255–63.
18 Weller RO, Djuanda E, Yow HY, Carare RO. Lymphatic drainage of the brain and the pathophysiology of neurological disease. *Acta Neuropathol* 2009; **117**: 1–14.
19 National Toxicology Program. NTP technical report on the toxicology and carcinogenesis studies of dimethyl vinyl chloride (L-chloro-2-methylpropene) (Cas No. 513-37-1) in F344/N rats and B6C3F1 mice (Gavage Studies) (NTP TR 316). National Toxicology Program, Research Triangle Park, North Carolina, 1986. [Cited 26 May 2012.] Available from URL: http://ntp.niehs.nih.gov/ntp/htdocs/lt_rpts/tr316.pdf.
20 National Toxicology Program. NTP technical report on the toxicology and carcinogenesis studies of glycidol (Cas No. 556-52-5) in F344/N rats and B6C3F1 mice (Gavage Studies) (NTP TR 374). National Toxicology Program, Research Triangle Park, North Carolina, 1990. [Cited 26 May 2012.] Available from URL: http://ntp.niehs.nih.gov/ntp/htdocs/LT_rpts/tr374.pdf.
21 Boffetta P, Burdorf A, Goldberg M, Merler E, Siemiatycki J. Towards the coordination of European research on the carcinogenic effects of asbestos. *Scand J Work Environ Health* 1998; **24**: 312–7.
22 Yano E, Wang ZM, Wang XR, Wang MZ, Lan YJ. Cancer mortality among workers exposed to amphibole-free chrysotile asbestos. *Am J Epidemiol* 2001; **154**: 538–43.
23 Donaldson K, Murphy FA, Duffin R, Poland CA. Asbestos, carbon nanotubes and the pleural mesothelium: a review of the hypothesis regarding the role of long fibre retention in the parietal pleura, inflammation and mesothelioma. *Part Fibre Toxicol* 2010; **7**: 5.
24 Poland CA, Duffin R, Kinloch I *et al.* Carbon nanotubes introduced into the abdominal cavity of mice show asbestos-like pathogenicity in a pilot study. *Nat Nanotechnol* 2008; **3**: 423–8.
25 Nagai H, Toyokuni S. Biopersistent fiber-induced inflammation and carcinogenesis: lessons learned from asbestos toward safety of fibrous nanomaterials. *Arch Biochem Biophys* 2010; **502**: 1–7.
26 Tossavainen A, Karjalainen A, Karhunen PJ. Retention of asbestos fibers in the human body. *Environ Health Perspect* 1994; **102**(Suppl 5): 253–5.
27 Miserocchi G, Sancini G, Mantegazza F, Chiappino G. Translocation pathways for inhaled asbestos fibers. *Environ Health* 2008; **7**: 4.
28 Goldsmith JR. Asbestos as a systemic carcinogen: the evidence from eleven cohorts. *Am J Ind Med* 1982; **3**: 341–8.
29 Noonan CW, Pfau JC, Larson TC, Spence MR. Nested case-control study of autoimmune disease in an asbestos-exposed population. *Environ Health Perspect* 2006; **114**: 1243–7.

Supporting Information

Additional Supporting Information may be found in the online version of this article:

Fig. S1. Estimation of the time of tumor onset.

Please note: Wiley-Blackwell are not responsible for the content or functionality of any supporting materials supplied by the authors. Any queries (other than missing material) should be directed to the corresponding author for the article.

doi: 10.1111/j.1349-7006.2012.02318.x

Cancer Science
The official journal of the Japanese Cancer Association JCA

Multi-walled carbon nanotubes translocate into the pleural cavity and induce visceral mesothelial proliferation in rats

Jiegou Xu,[1,2] Mitsuru Futakuchi,[2] Hideo Shimizu,[3] David B. Alexander,[1] Kazuyoshi Yanagihara,[4] Katsumi Fukamachi,[2] Masumi Suzui,[2] Jun Kanno,[5] Akihiko Hirose,[6] Akio Ogata,[7] Yoshimitsu Sakamoto,[7] Dai Nakae,[7] Toyonori Omori[8] and Hiroyuki Tsuda[1,9]

[1]Laboratory of Nanotoxicology Project, Nagoya City University, Nagoya; [2]Department of Molecular Toxicology; [3]Core Laboratory, Nagoya City University Graduate School of Medical Sciences, Nagoya; [4]Department of Life Sciences, Yasuda Women's University Faculty of Pharmacy, Hiroshima; [5]Division of Cellular and Molecular Toxicology; [6]Division of Risk Assessment, National Institute of Health Sciences, Tokyo; [7]Department of Pharmaceutical and Environmental Sciences, Tokyo Metropolitan Institute of Public Health, Tokyo; [8]Department of Health Care Policy and Management, Nagoya City University Graduate School of Medical Sciences, Nagoya, Japan

(Received July 17, 2012/Revised August 20, 2012/Accepted August 22, 2012/Accepted manuscript online August 31, 2012/Article first published online October 10, 2012)

Multi-walled carbon nanotubes have a fibrous structure similar to asbestos and induce mesothelioma when injected into the peritoneal cavity. In the present study, we investigated whether carbon nanotubes administered into the lung through the trachea induce mesothelial lesions. Male F344 rats were treated with 0.5 mL of 500 μg/mL suspensions of multi-walled carbon nanotubes or crocidolite five times over a 9-day period by intrapulmonary spraying. Pleural cavity lavage fluid, lung and chest wall were then collected. Multi-walled carbon nanotubes and crocidolite were found mainly in alveolar macrophages and mediastinal lymph nodes. Importantly, the fibers were also found in the cell pellets of the pleural cavity lavage, mostly in macrophages. Both multi-walled carbon nanotube and crocidolite treatment induced hyperplastic proliferative lesions of the visceral mesothelium, with their proliferating cell nuclear antigen indices approximately 10-fold that of the vehicle control. The hyperplastic lesions were associated with inflammatory cell infiltration and inflammation-induced fibrotic lesions of the pleural tissues. The fibers were not found in the mesothelial proliferative lesions themselves. In the pleural cavity, abundant inflammatory cell infiltration, mainly composed of macrophages, was observed. Conditioned cell culture media of macrophages treated with multi-walled carbon nanotubes and crocidolite and the supernatants of pleural cavity lavage fluid from the dosed rats increased mesothelial cell proliferation *in vitro*, suggesting that mesothelial proliferative lesions were induced by inflammatory events in the lung and pleural cavity and likely mediated by macrophages. In conclusion, intrapulmonary administration of multi-walled carbon nanotubes, like asbestos, induced mesothelial proliferation potentially associated with mesothelioma development. (*Cancer Sci* 2012; 103: 2045–2050)

Multi-walled carbon nanotubes (MWCNT) are structurally composed of cylinders rolled up from several layers of graphite sheets. They are several to tens of nanometers in diameter and several to tens of micrometers in length. This high length to diameter aspect ratio, a characteristic shared with asbestos fibers, has led to concern that exposure to MWCNT might cause asbestos-like lung diseases, such as lung fibrosis, lung cancer, pleural plaque and malignant mesothelioma.[1–6]

Pleural plaque and malignant mesothelioma are characteristic lesions in asbestos-exposed humans. Although fiber dimensions, biopersistence, oxidative stress and inflammation have all been implicated,[7–12] the exact mechanisms of pleural pathogenesis are unclear. According to a pathogenesis paradigm suggested by Donaldson *et al.*,[2] asbestos fibers penetrate into the pleural cavity from the alveoli and deposit in the pleural tissue. Unlike spherical particles, fibrous materials such as asbestos are not cleared effectively from the pleural cavity, resulting in deposition of the fibers in the parietal pleura. This deposition, in turn, causes frustrated phagocytosis-induced pro-inflammatory, genotoxic and mitogenic responses in the deposition sites.[2]

Administration of MWCNT into the peritoneal cavity or scrotum in animals has been reported to induce mesothelial lesions, similar to those observed in asbestos cases.[13–15] The induction of mesothelioma in the peritonum is dose dependent, and is observed with as low as 3 μg/mouse in p53 heterozygous mice.[16] These studies suggest a potential risk that inhaled MWCNT might lead to pleural mesothelioma. However, actual experimental evidence demonstrating induction of pleural mesothelioma by inhaled MWCNT fibers has not yet been shown. It has been shown that inhaled MWCNT induced subpleural fibrosis with macrophage aggregates on the surface of the visceral pleura.[17] Notably, some of these macrophages contained MWCNT fibers. In addition, penetration of MWCNT administrated by pharyngeal aspiration into the pleural cavity was observed.[18] and intrapleural injection of 5 μg/mouse of MWCNT has been shown to lead to sustained inflammation and length-dependent retention of MWCNT in the pleural cavity.[19] Accordingly, direct interaction of MWCNT with the mesothelial tissue is postulated as an early pathogenic event.

In the present study, to examine whether MWCNT translocate into the pleural cavity and cause inflammation leading to proliferative change of the mesothelial tissue, we administered relatively high doses (five doses at 250 μg/rat) of two MWCNT samples (MWCNT-N and MWCNT-M) to the rat lung by intrapulmonary spraying (IPS)/intratracheal instillation; crocidolite (CRO; one kind of asbestos fiber) was used as a positive control. Intrapulmonary spraying has been shown to be an efficient method to deliver particle materials deep into the lung.[20–24] Our results demonstrated that MWCNT, like asbestos, translocated from the lung into the pleural cavity and induced inflammatory responses in the pleural cavity and, importantly, hyperplastic visceral mesothelial proliferation. These findings are important in understanding whether MWCNT have the potential to cause asbestos-like pleural lesions.

[9]To whom correspondence should be addressed.
E-mail: htsuda@phar.nagoya-cu.ac.jp

doi: 10.1111/cas.12005

Materials and Methods

Animals. Eight-week-old male F344 rats were purchased from Charles River Japan Inc. (Kanagawa, Japan). The animals were housed in the Animal Center of Nagoya City University Medical School and maintained on a 12 h light/12 h dark cycle, and received Oriental MF basal diet (Oriental Yeast Co. Ltd, Tokyo, Japan) and water *ad libitum*. The study was conducted according to the Guidelines for the Care and Use of Laboratory Animals of Nagoya City University Medical School and the experimental protocol was approved by the Institutional Animal Care and Use Committee (H22M-19).

Preparation of MWCNT and CRO suspensions. The MWCNT investigated were MWCNT-N (Nikkiso Co., Ltd, Tokyo, Japan) and MWCNT-7 (Mitsui Chemicals Inc., Tokyo, Japan; designated as MWCNT-M). Crocidolite (Union for International Cancer Control grade) was from the National Institute of Health Sciences of Japan stocks. Ten milligrams of MWCNT-N or MWCNT-M were suspended in 20 mL of saline containing 0.1% Tween 20 and homogenized for 1 min four times at 3000 r.p.m. in a Polytron PT1600E benchtop homogenizer (Kinematika AG, Littau, Switzerland). The suspensions were sonicated for 30 min shortly before use to minimize aggregation. The CRO suspension was prepared similarly, but without homogenization. The concentration of the MWCNT and CRO suspensions was 500 μg/mL. The lengths of MWCNT and CRO in the suspensions were determined using a digital map meter (Comcureve-9 Junior; Koizumi Sokki MFG. Co., Ltd, Nigata, Japan) on scanning electron microscope (SEM) photos. The SEM observation and length distributions of MWCNT and CRO are shown in Fig. S1A,B. To count the fiber number, 500 μg/mL suspensions of MWCNT-N, MWCNT-M and CRO were diluted 1:1000 with deionized water and 0.5 μL of the diluted suspensions was loaded onto clean glass slides and dried in a micro oven at 480°C for 1 min. The fiber number on the slides was counted under a polarized light microscope (PLM) (Olympus BX51N-31P-O PLM, Tokyo, Japan) (PLM detects all fibers longer than 200 nm). The results are shown in Fig. S1C.

Intrapulmonary spraying of MWCNT and CRO into the lung and pleural cavity lavage (PCL). We used the intrapulmonary spraying technique that was developed in our laboratory.[24] Briefly, rats were anaesthetized using isoflurane; the mouth was fully opened with the tongue gently held and the nozzle of a microsprayer (series IA-1B Intratracheal Aerosolizer; Penn-century, Philadelphia, PA, USA) was inserted into the trachea through the larynx and 0.5 mL suspension was sprayed into the lungs synchronizing with spontaneous respiratory inhalation. We confirmed that the dosed materials were distributed deep into the lung tissue and reached most of the terminal alveoli without causing obvious respiratory distress.

Ten-week-old male Fisher 344 rats were divided into four groups of six animals each and given 0.5 mL of saline containing 0.1% Tween 20 or 500 μg/mL MWCNT-N, MWCNT-M or CRO suspension by IPS once every other day five times over a 9-day period. The total amount of fibers administered was 1.25 mg/rat. Six hours after the last IPS, the rats were placed under deep isoflurane anesthesia; a small incision was made in the abdominal wall, the pleural cavity was injected with 10 mL of ice cold RPMI 1640 through the diaphragm, and the lavage fluid was collected by syringe. The rats were then killed by exsanguination from the inferior vena cava and the major organs, including the lung, chest wall, brain, liver, kidney, spleen and mediastinal lymph nodes, were fixed in 4% paraformaldehyde and processed for histological examination.

Analysis of inflammatory reaction in the pleural cavity. Cells in the lavage fluid were counted using a hemocytometer (Erma Co., Ltd, Tokyo, Japan), and the cellular fraction was then isolated by centrifugation at 200*g* for 5 min at 4°C. Cell pellets collected from three rats were combined (generating a total of two cell pellets per group), fixed in 4% paraformaldehyde and processed for histological examination. Total protein in the supernatants of each of the lavage fluids was determined using the Pierce BCA Protein Assay Kit (Thermo Scientific, Rockford, IL, USA) and the supernatants were then concentrated by centrifugation in Vivaspin 15 concentrators (Sartorius Stedium Biotech, Goettingen, Germany) at 1500*g* for 30 min at 4°C and used for *in vitro* cell proliferation assays.

Light microscopy and PLM. Haematoxylin–eosin (H&E)-stained slides of the lung tissues and cellular pellets of the PCL were used to observe MWCNT-N, MWCNT-M and CRO fibers with PLM at ×1000 magnification. The exact localization of the illuminated fibers was confirmed in the same H&E-stained sections after removing the polarizing filter.

Scanning electron microscopy. The H&E-stained slides of the lung tissue and PCL pellets were immersed in xylene for 3 days to remove the cover glass, then immersed in 100% ethanol for 10 min to remove the xylene and air-dried for 2 h at room temperature. The slides were then coated with platinum for viewing using a scanning electronic microscope (SEM) (Model S-4700 Field Emission SEM; Hitachi High Technologies Corporation, Tokyo, Japan) at 5–10 kV.

Immunohistochemistry and Azan–Mallory staining. CD68, proliferating cell nuclear antigen (PCNA) and mesothelin/Erc were detected using antirat CD68 antibodies (BMA Biomedicals, Augst, Switzerland), anti-PCNA monoclonal antibodies (Clone PC10; Dako Japan Inc., Tokyo, Japan) and antirat C-ERC/mesothelin polyclonal antibodies (Immuno-Biological Laboratories Co., Ltd, Gunma, Japan). The CD68, PCNA and C-ERC/mesothelin antibodies were diluted 1:100, 1:200 and 1:1000, respectively, in blocking solution and applied to deparaffinized slides. The slides were incubated at 4°C overnight and then incubated for 1 h with biotinylated species-specific secondary antibodies diluted 1:500 (Vector Laboratories, Burlingame, CA, USA) and visualized using avidin-conjugated horseradish peroxidase complex (ABC kit; Vector Laboratories). Azan–Mallory staining was used to visualize collagen fibers.

***In vitro* exposure and preparation of conditioned macrophage culture media.** The induction and preparation of primary alveolar macrophages (PAM) has been described previously.[24] PAM were seeded into 6 cm culture dishes at 2×10^6 cells per well in 10% FBS RPMI 1640. After overnight incubation, the culture media was refreshed and MWCNT-N, MWCNT-M or CRO suspensions were added to the cells to a final concentration of 10 μg/mL. The cells were then incubated for another 24 h. The conditioned macrophage culture media was then collected for *in vitro* cell proliferation assays.

***In vitro* cell proliferation assay.** Human mesothelioma cells, TCC-MESO1, derived from a patient in the Tochigi Cancer Center,[25] were seeded into 96-well culture plates at 2×10^3 cells per well in 10% FBS RPMI 1640. After overnight incubation, the cells were serum-starved for 24 h. The media was changed to 100 μL of the concentrated supernatants of the PCL or conditioned macrophage culture media and incubated for 72 h. The relative cell number was then determined using the Cell Counting Kit-8 (Dojindo Molecular Technologies, Rockville, MD, USA) according to the manufacturer's instruction.

Statistical analysis. Statistical analysis was performed using ANOVA. The statistical significance was analyzed using a two-tailed Student's *t*-test. A *P*-value of <0.05 was considered to be significant.

Results

Translocation of MWCNT and CRO fibers into the pleural cavity. The cell pellets of the PCL were used to examine whether

doi: 10.1111/cas.12005

the MWCNT or CRO fibers were present in the pleural cavity. We first screened the H&E-stained PCL cell pellet slides using PLM. The exact localization of the fibers was confirmed using SEM of the same slide sections. MWCNT-N, MWCNT-M and CRO fibers were present in PCL cell pellets, with most of the fibers in macrophage-like cells (Fig. 1a–c) with very few fibers located in the intercellular space or on cell surfaces (data not shown). Immunohistochemistry with CD68, a macrophage marker, showed that MWCNT and CRO fibers were mainly found in macrophages (Fig. 1d,e).

In tissue sections, MWCNT and CRO fibers were mainly detected in focal granulomatous lesions in the alveoli and in alveolar macrophages. Fibers were also found in the mediastinal lymph nodes, and a few fibers were detected in liver sinusoid cells, blood vessel wall cells in the brain, renal tubular cells and spleen sinus and macrophages (data not shown). We detected only a few fibers penetrating directly from the lung to the pleural cavity through the visceral pleura (Fig. S2) and did not find any fibers in the parietal pleura.

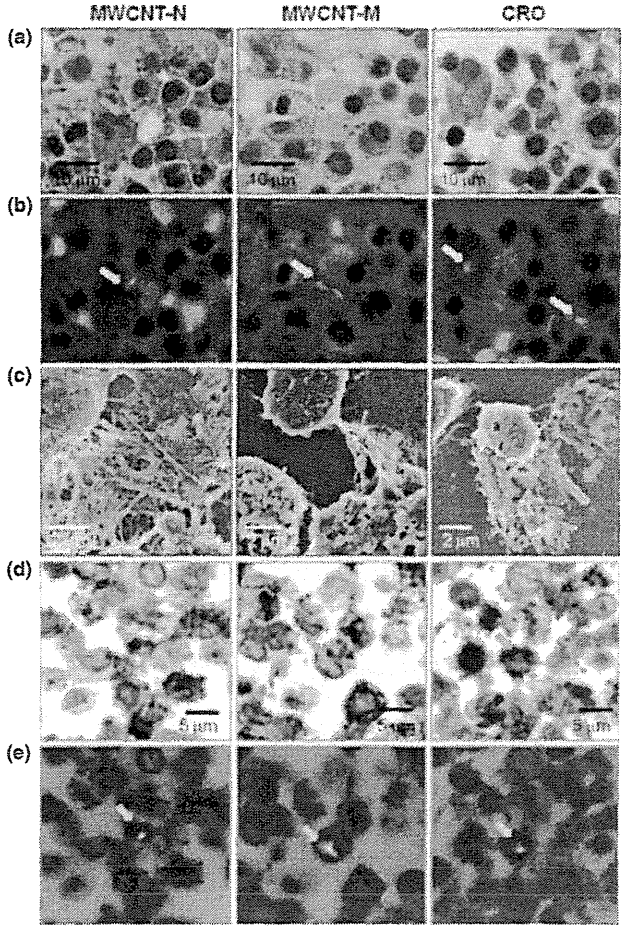

Fig. 1. Existence of multi-walled carbon nanotubes (MWCNT)-N, MWCNT-M and crocidolite (CRO) fibers in the cell pellets of the pleural cavity lavage (PCL). (a) Images of H&E-stained slides of the cell pellets of the PCL treated with MWCNT-N, MWCNT-M and CRO fibers. (b) Polarized light microscope (PLM) images of the same view areas shown in (a). (c) Scanning electron microscope observation showed the existence of the MWCNT and CRO fibers in the cell pellets of the PCL. (d) CD68 immunostaining of the PCL cell pellet slides. (e) PLM observation of the same view areas shown in (d) indicate that MWCNT and CRO fibers were present in the CD68-positive macrophages. Arrows indicate MWCNT-N, MWCNT-M and CRO fibers.

Induction of visceral mesothelial proliferation. Hyperplastic visceral mesothelial proliferation (HVMP) was clearly observed in all of the MWCNT and CRO treated groups. The HVMP lesions were composed of mesothelial cells with cuboidal appearance and increased size and density lining the visceral pleural tissue. Various degrees of lung inflammation and fibrous thickening were observed underneath the HVMP lesions (Fig. 2a, panel A). The PCNA immunostaining showed proliferating mesothelial cells within the HVMP lesions (Fig. 2a, panel B). The PCNA indices of the visceral mesothelium were increased approximately 10-fold in all the MWCNT and CRO treated groups compared with the control group

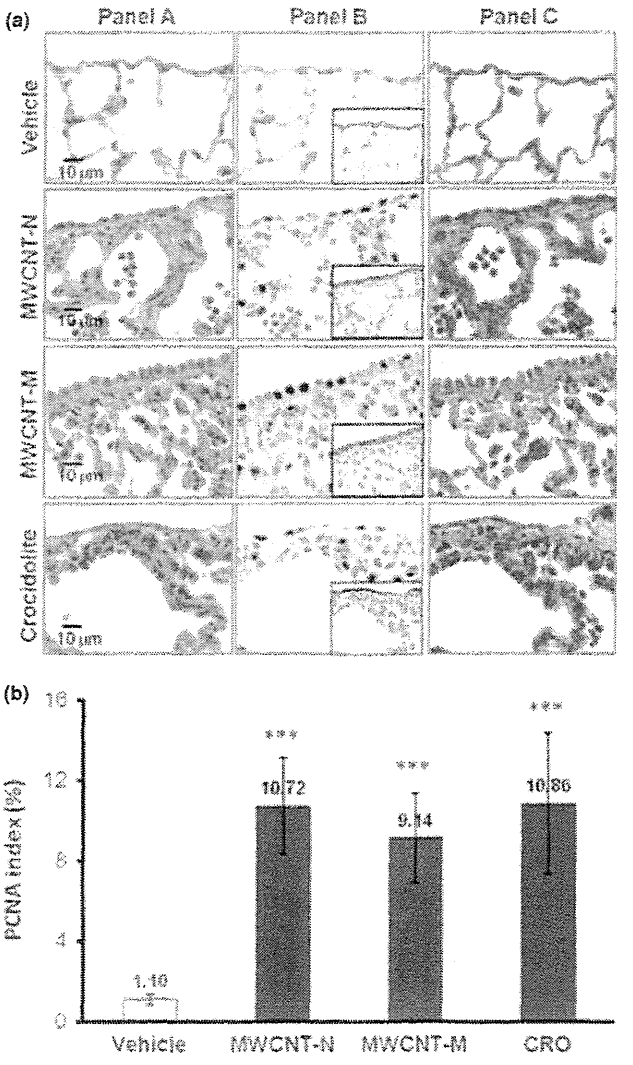

Fig. 2. Induction of visceral mesothelial cell proliferation lesions by treatment with multi-walled carbon nanotubes (MWCNT)-N, MWCNT-M or crocidolite (CRO). (a) Serial sections were prepared and stained with H&E, proliferating cell nuclear antigen (PCNA), Erc/mesothelin and Azan–Mallory's collagen staining. Panel A: increase in enlarged visceral mesothelial cells with cuboidal shapes in the MWCNT-N, MWCNT-M and CRO treated groups. Panel B: PCNA-positive cells are clearly increased in the dosed groups. The inserts are immunostained with Erc/mesothelin and show the lining of the mesothelium. Panel C: Azan–Mallory's staining; sub-pleural collagenous fibrosis is present under the mesothelial cell proliferation lesions. (b) PCNA index, expressed as the percentage of PCNA-positive cells of the total number of visceral mesothelial cells per slide. ***$P < 0.001$.

(Fig. 2b). Azan–Mallory staining showed increases in collagen fibers underneath the HVMP lesions (Fig. 2a, panel C). Fibers were not found within the HVMP lesions themselves. Alveolar macrophages with phagocytosed MWCNT or CRO fibers were frequently observed near the HVMP lesions (Fig. S3). Proliferation and other lesions of the parietal mesothelium were not observed.

Inflammatory cell infiltration in the pleural cavity. Both MWCNT and CRO treatment resulted in inflammatory reactions in the pleural cavity. The total number of cells, composed mostly of macrophages, neutrophils and lymphocytes, in the PCL in the MWCNT and CRO treated groups was significantly increased compared with the control group (Fig. 3a). As can be calculated from Fig. 3(a,b), macrophages accounted for a large part of the increase of the total cell number in the PCL, although the number of neutrophils and lymphocytes also increased. Overall, the proportion of macrophages in the cell pellets of the PCL was increased, while those of neutrophils and lymphocytes were decreased (Fig. 3b). MWCNT or CRO treatment also significantly increased the total protein level in the PLC (Fig. 3c). The proportion of cells in the PCL pellets positive for Mesothelin/Erc, a mesothelial cell marker, was 0.53–1.02%, and no intergroup difference was observed (data not shown). These data indicate that the increased cell number in the pleural cavity of the rats treated with MWCNT or CRO resulted from inflammatory cell effusion, not from mesothelial cell shedding of the pleural tissue. Many macrophages in the PCL contained MWCNT or CRO fibers.

Mesothelial cell proliferation assay *in vitro*. To examine whether inflammatory reactions, especially those mediated by macrophages, exert proliferative effects on mesothelial cells, we examined the effects of conditioned macrophage culture medium on mesothelial cell proliferation *in vitro*. The conditioned culture media of macrophages exposed to MWCNT-N, MWCNT-M or CRO significantly increased the proliferation of the human mesothelioma cell line TCC-MESO1. The concentrated supernatants of the PCL taken from the rats treated with MWCNT-N, MWCNT-M or CRO exhibited similar effects (Fig. 4). These results indicate that factors in the PCL, possibly secreted by alveolar and pleural macrophages, are able to cause mesothelial cell proliferation.

Discussion

In the present study, we compared the pleural translocation of MWCNT and CRO and examined the mesothelial lesions they induced. Our data demonstrate that after deposition in the lung, MWCNT, like CRO, translocated into the pleural cavity, mainly in pleural macrophages. Both MWCNT and CRO treatment also caused hyperplastic visceral mesothelial proliferation and marked pleural inflammation.

This is the first report to show that MWCNT administered into the rat lung causes mesothelial proliferative lesions. Adamson *et al.*[26] reported that intratracheal instillation of asbestos in mice induced pleural mesothelial cell proliferation within several days; the degree of pleural mesothelial cell proliferation did not appear to correlate with the localization of asbestos fibers in the pleura.[27] Similarly, we did not find fibers within the HVMP lesions. Thus, our findings suggest that HVMP lesions do not appear to be directly induced by the deposited MWCNT or CRO fibers. Also, *in vitro* exposure to MWCNT and CRO fibers did not lead to proliferation of TCC-MESO1 cells, but rather to cell death (Fig. S4). It has been reported that macrophages play a significant role in mesothelial cell proliferation caused by asbestos exposure and surgical injury,[28–31] and that the conditioned medium of macrophages

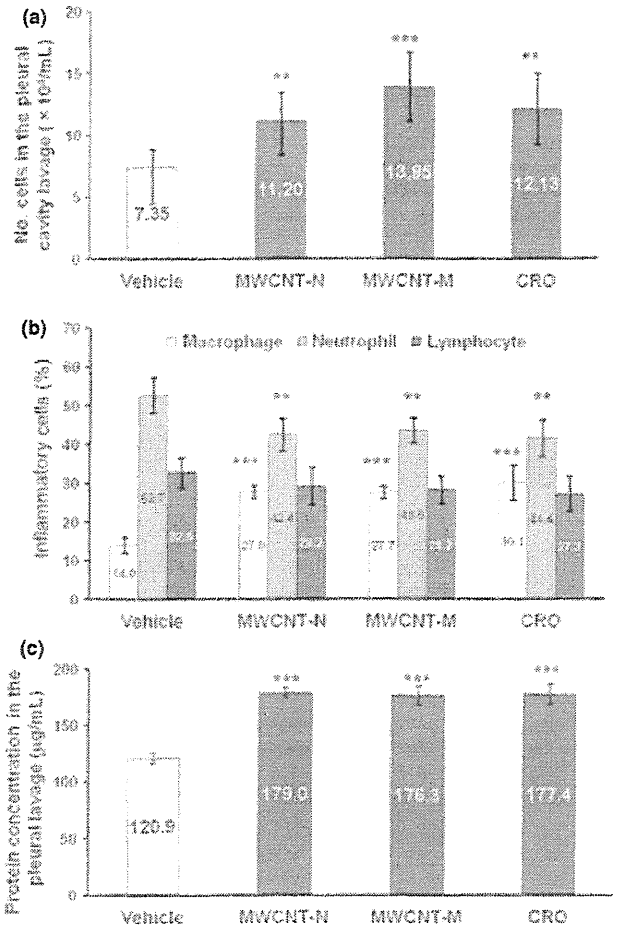

Fig. 3. Inflammatory reaction in the pleural cavity. (a) The number of leukocytes in the pleural cavity lavage (PCL) of rats treated with multi-walled carbon nanotubes (MWCNT) and crocidolite (CRO). (b) The proportion of macrophages, neutrophils and lymphocytes in the cell pellets of the PCL. Total cell number and cell numbers of macrophages, neutrophils and lymphocytes in 10 randomly chosen fields (×400) were counted. (c) Protein concentration in the supernatants of the PCL. $^{**}P < 0.01$; $^{***}P < 0.001$.

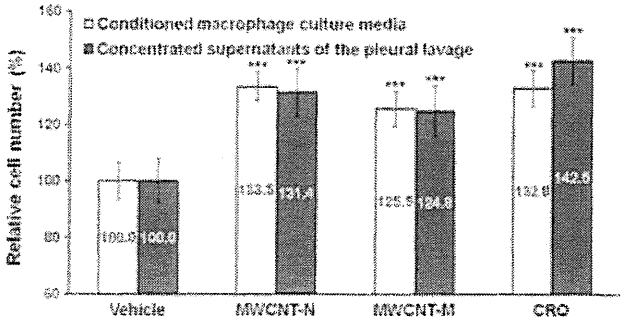

Fig. 4. Effect of conditioned macrophage culture media and the supernatants of the pleural cavity lavage (PCL) on mesothelial cell proliferation *in vitro*. The conditioned culture media of macrophages treated with multi-walled carbon nanotubes (MWCNT)-N, MWCNT-M or crocidolite (CRO) significantly increased the cell proliferation of TCC-MESO1. The concentrated supernatants of the PCL from the rats treated with MWCNT-N, MWCNT-M or CRO had similar effects. $n = 6$. $^{***}P < 0.001$.

doi: 10.1111/cas.12005

exposed to MWCNT promotes mesothelial cell proliferation *in vitro*.[30] Activated macrophages secrete a panel of growth factors and cytokines to regulate cell proliferation, which can augment transformation of mesothelial cells.[28,30,32,33] Our observations that mesothelial cell proliferation is enhanced by conditioned macrophage culture media and by the supernatants of pleural cavity lavage are consistent with these results, although the factors that are involved need to be identified.

Translocation of asbestos[34,35] and MWCNT[18] fibers from the lung to the pleural cavity has been found in rodents. This translocation also probably occurs in humans since asbestos fibers have been detected in human pleural lesions.[36] However, the mechanism and route of translocation are unclear. It has been suggested that penetration through the visceral pleura, possibly driven by increased pulmonary interstitial pressure and assisted by enhanced permeability of the visceral pleura due to asbestos-induced inflammation might be a major route.[37] In the present study, only a few MWCNT and CRO fibers were observed penetrating through the visceral pleura, and a large number of the fibers in the pleural cavity was observed in macrophages. We also observed frequent deposition of MWCNT and CRO in the mediastinal lymph nodes, mostly phagocytosed by macrophages. These results suggest that a probable route of translocation of the fibers is lymphatic flow. Inflammation in the pleural cavity is probably a defense response against translocated fibers. Murphy *et al.*[19] reported that intrapleural injection of 5 μg/mouse of long MWCNT or asbestos initiated sustained inflammation, including increased granulocyte number and protein level, in the pleural cavity. Thus, the observed proliferation of visceral mesothelial cells in the present study is probably caused by inflammatory reactions both in the lung and in the pleural cavity. In the present study, no MWCNT or crosidolite fibers or lesions were observed in the parietal pleura. This is possibly due to the short experimental period and limited amount of fibers in the pleural cavity, which would result in little inflammation in the parietal pleura.

Currently, the exposure level to MWCNT in the workplace is unknown and there are no administrational regulations for the occupational exposure limit for MWCNT. In November 2010, the National Institute of Occupational Safety and Health (NIOSH) released a non-official carbon nanotube exposure limit for peer review. The recommended exposure limit in the air was set at 7 μg/m^3.[38] Previously, we used a total dose of 1.25 mg/rat of titanium dioxide over a 9-day period and identified factors involved in titanium dioxide-induced lung lesions.[24] In the present study, we used the same protocol for the purpose of induction of observable pleural lesions and inflammation in the pleural cavity as well to ensure the presence of a detectable number of fibers in the pleural cavity after short-term administration; this dose was higher than the NIOSH exposure limit. Time- and dose-dependent experiments are needed in future studies, and further investigation is also required to elucidate cytokines and other factors that cause parietal mesothelial proliferation in animal models that are more relevant to humans.

The IPS/intratracheal instillation is a widely used method to evaluate the respiratory toxicity of particles. It should be noted that IPS/intratracheal instillation is a non-physiological method and possibly affects the migration and distribution of particles in the lung due to the pressure from spraying. However, IPS/intratracheal instillation is relevant for identifying factors to be examined using long-term, more physiologically relevant methods of CNT administration.

In summary, MWCNT and CRO fibers were found to translocate from the lung to the pleural cavity after intrapulmonary administration. Importantly, MWCNT and CRO treatment caused visceral mesothelial cell proliferation and inflammation in the pleural cavity. This mesothelial proliferation was plausibly induced by inflammatory events in the lung and pleural cavity and mediated primarily by macrophages. The similarity between MWCNT-N, MWCNT-M and CRO in translocation to the pleural cavity, induction of pleural cavity inflammation and induction of visceral pleural mesothelial proliferation suggests that MWCNT might cause asbestos-like pleural lesions.

Acknowledgments

This work was supported by Health and Labour Sciences Research Grants (Research on Risk of Chemical Substance 21340601) (grant numbers H19-kagaku-ippan-006, H22-kagaku-ippan-005).

Disclosure Statement

The authors have no conflict of interest.

References

1 Bonner JC. Nanoparticles as a potential cause of pleural and interstitial lung disease. *Proc Am Thorac Soc* 2010; **7**: 138–41.
2 Donaldson K, Murphy FA, Duffin R *et al.* Asbestos, carbon nanotubes and the pleural mesothelium: a review of the hypothesis regarding the role of long fibre retention in the parietal pleura, inflammation and mesothelioma. *Part Fibre Toxicol* 2010; **7**: 5.
3 Johnston HJ, Hutchison GR, Christensen FM *et al.* A critical review of the biological mechanisms underlying the *in vivo* and *in vitro* toxicity of carbon nanotubes: the contribution of physico-chemical characteristics. *Nanotoxicology* 2010; **4**: 207–46.
4 Nagai H, Toyokuni S. Biopersistent fiber-induced inflammation and carcinogenesis: lessons learned from asbestos toward safety of fibrous nanomaterials. *Arch Biochem Biophys* 2010; **502**: 1–7.
5 Pacurari M, Castranova V, Vallyathan V. Single- and multi-wall carbon nanotubes versus asbestos: are the carbon nanotubes a new health risk to humans? *J Toxicol Environ Health A* 2010; **73**: 378–95.
6 Tsuda H, Xu J, Sakai Y *et al.* Toxicology of engineered nanomaterials – a review of carcinogenic potential. *Asian Pac J Cancer Prev* 2009; **10**: 975–80.
7 Barrett JC. Cellular and molecular mechanisms of asbestos carcinogenicity: implications for biopersistence. *Environ Health Perspect* 1994; **102** (Suppl 5): 19–23.
8 Miller BG, Searl A, Davis JM *et al.* Influence of fibre length, dissolution and biopersistence on the production of mesothelioma in the rat peritoneal cavity. *Ann Occup Hyg* 1999; **43**: 155–66.
9 Okada F. Beyond foreign-body-induced carcinogenesis: impact of reactive oxygen species derived from inflammatory cells in tumorigenic conversion and tumor progression. *Int J Cancer* 2007; **121**: 2364–72.
10 Stanton MF, Wrench C. Mechanisms of mesothelioma induction with asbestos and fibrous glass. *J Natl Cancer Inst* 1972; **48**: 797–821.
11 Walker C, Everitt J, Barrett JC. Possible cellular and molecular mechanisms for asbestos carcinogenicity. *Am J Ind Med* 1992; **21**: 253–73.
12 Yang H, Testa JR, Carbone M. Mesothelioma epidemiology, carcinogenesis, and pathogenesis. *Curr Treat Options Oncol* 2008; **9**: 147–57.
13 Poland CA, Duffin R, Kinloch I *et al.* Carbon nanotubes introduced into the abdominal cavity of mice show asbestos-like pathogenicity in a pilot study. *Nat Nanotechnol* 2008; **3**: 423–8.
14 Sakamoto Y, Nakae D, Fukumori N *et al.* Induction of mesothelioma by a single intrascrotal administration of multi-wall carbon nanotube in intact male Fischer 344 rats. *J Toxicol Sci* 2009; **34**: 65–76.
15 Takagi A, Hirose A, Nishimura T *et al.* Induction of mesothelioma in p53+/− mouse by intraperitoneal application of multi-wall carbon nanotube. *J Toxicol Sci* 2008; **33**: 105–16.
16 Takagi A, Hirose A, Futakuchi M *et al.* Dose-dependent mesothelioma induction by intraperitoneal administration of multi-wall carbon nanotubes in p53 heterozygous mice. *Cancer Sci* 2012; **103**: 1440–4.
17 Ryman-Rasmussen JP, Cesta MF, Brody AR *et al.* Inhaled carbon nanotubes reach the subpleural tissue in mice. *Nat Nanotechnol* 2009; **4**: 747–51.
18 Mercer RR, Hubbs AF, Scabilloni JF *et al.* Distribution and persistence of pleural penetrations by multi-walled carbon nanotubes. *Part Fibre Toxicol* 2010; **7**: 28.

19 Murphy FA, Poland CA, Duffin R *et al.* Length-dependent retention of carbon nanotubes in the pleural space of mice initiates sustained inflammation and progressive fibrosis on the parietal pleura. *Am J Pathol* 2011; **178**: 2587–600.
20 Oka Y, Mitsui M, Kitahashi T *et al.* A reliable method for intratracheal instillation of materials to the entire lung in rats. *J Toxicol Pathol* 2006; **19**: 107–9.
21 Jackson P, Hougaard KS, Boisen AM *et al.* Pulmonary exposure to carbon black by inhalation or instillation in pregnant mice: effects on liver DNA strand breaks in dams and offspring. *Nanotoxicology* 2012; **6**: 486–500.
22 Morimoto Y, Hirohashi M, Ogami A *et al.* Pulmonary toxicity of well-dispersed multi-wall carbon nanotubes following inhalation and intratracheal instillation. *Nanotoxicology* 2012; **6**: 587–99.
23 Ogami A, Yamamoto K, Morimoto Y *et al.* Pathological features of rat lung following inhalation and intratracheal instillation of C(60) fullerene. *Inhal Toxicol* 2011; **23**: 407–16.
24 Xu J, Futakuchi M, Iigo M *et al.* Involvement of macrophage inflammatory protein 1alpha (MIP1alpha) in promotion of rat lung and mammary carcinogenic activity of nanoscale titanium dioxide particles administered by intrapulmonary spraying. *Carcinogenesis* 2010; **31**: 927–35.
25 Yanagihara K, Tsumuraya M, Takigahira M *et al.* An orthotopic implantation mouse model of human malignant pleural mesothelioma for *in vivo* photon counting analysis and evaluation of the effect of S-1 therapy. *Int J Cancer* 2010; **126**: 2835–46.
26 Adamson IY, Bakowska J, Bowden DH. Mesothelial cell proliferation after instillation of long or short asbestos fibers into mouse lung. *Am J Pathol* 1993; **142**: 1209–16.
27 Sekhon H, Wright J, Churg A. Effects of cigarette smoke and asbestos on airway, vascular and mesothelial cell proliferation. *Int J Exp Pathol* 1995; **76**: 411–8.
28 Adamson IY, Prieditis H, Young L. Lung mesothelial cell and fibroblast responses to pleural and alveolar macrophage supernatants and to lavage fluids from crocidolite-exposed rats. *Am J Respir Cell Mol Biol* 1997; **16**: 650–6.
29 Li XY, Lamb D, Donaldson K. Mesothelial cell injury caused by pleural leukocytes from rats treated with intratracheal instillation of crocidolite asbestos or *Corynebacterium parvum*. *Environ Res* 1994; **64**: 181–91.
30 Murphy FA, Schinwald A, Poland CA *et al.* The mechanism of pleural inflammation by long carbon nanotubes: interaction of long fibres with macrophages stimulates them to amplify pro-inflammatory responses in mesothelial cells. *Part Fibre Toxicol* 2012; **9**: 8.
31 Mutsaers SE, Whitaker D, Papadimitriou JM. Stimulation of mesothelial cell proliferation by exudate macrophages enhances serosal wound healing in a murine model. *Am J Pathol* 2002; **160**: 681–92.
32 Lechner JF, LaVeck MA, Gerwin BI *et al.* Differential responses to growth factors by normal human mesothelial cultures from individual donors. *J Cell Physiol* 1989; **139**: 295–300.
33 Wang Y, Faux SP, Hallden G *et al.* Interleukin-1beta and tumour necrosis factor-alpha promote the transformation of human immortalised mesothelial cells by erionite. *Int J Oncol* 2004; **25**: 173–8.
34 Choe N, Tanaka S, Xia W *et al.* Pleural macrophage recruitment and activation in asbestos-induced pleural injury. *Environ Health Perspect* 1997; **105** (Suppl 5): 1257–60.
35 Vialla JR, Raybuad F, Passarel M *et al.* Pleural migration of chrysotile fibers after intratracheal injection in rats. *Arch Environ Health* 1986; **41**: 282–6.
36 Kohyama N, Suzuki Y. Analysis of asbestos fibers in lung parenchyma, pleural plaques, and mesothelioma tissues of North American insulation workers. *Ann N Y Acad Sci* 1991; **643**: 27–52.
37 Miserocchi G, Sancini G, Mantegazza F *et al.* Translocation pathways for inhaled asbestos fibers. *Environ Health* 2008; **7**: 4.
38 NIOSH. Occupational exposure to carbon nanotubes and nanofibers. *Curr Intelligence Bull* 2010; **161-A**: 1–149.

Supporting Information

Additional Supporting Information may be found in the online version of this article:

Fig. S1. Characterization of multi-walled carbon nanotubes and crocidolite fibers in the suspensions.
Fig. S2. SEM observation of multi-walled carbon nanotubes and crocidolite fibers in the visceral pleura.
Fig. S3. Inflammation and fibrosis in the lung.
Fig. S4. Cytotoxicity of multi-walled carbon nanotubes and crocidolite to TCC-MESO1 cells *in vitro*.

doi: 10.1111/cas.12005

Circulating MicroRNAs in Serum of Human K-*ras* Oncogene Transgenic Rats With Pancreatic Ductal Adenocarcinomas

Setsuko Yabushita, MS, Katsumi Fukamachi, PhD,† Hajime Tanaka, MD, PhD,‡ Kayo Sumida, PhD,* Yoshihito Deguchi, DVM,* Tokuo Sukata, PhD,* Satoshi Kawamura, PhD,* Satoshi Uwagawa, PhD,* Masumi Suzui, MD, PhD,† and Hiroyuki Tsuda, MD, PhD§*

Objectives: Novel biomarkers for pancreatic ductal adenocarcinoma (PDAC) are urgently needed because of its poor prognosis. We have previously established an animal model for human PDAC using transgenic rats in which expression of a human K-*ras*^{G12V} oncogene is regulated by the *Cre/lox* system. Using this model, we searched for candidate circulating microRNAs (miRNAs) for use as novel clinical diagnostic biomarkers for PDAC.

Methods: Rats bearing PDACs were generated using our model. MicroRNA expression in serum and pancreatic tissues of PDAC and control rats was compared by microarray analysis. Rat serum levels of 28 miRNAs identified by microarray analysis and 4 miRNAs previously reported to be high in plasma of PDAC patients were quantified by real-time quantitative reverse transcription polymerase chain reaction.

Results: Quantification by real-time quantitative polymerase chain reaction revealed that miR-155, miR-21, and miR-210 were higher in serum of PDAC rats, similar to plasma of patients with PDAC. In addition, miR-18a, miR-203, miR-30b-5p, miR-31, miR-369-5p, miR-376a, and miR-541 were higher and miR-375 was lower in the serum of PDAC rats.

Conclusion: We identified 4 previously unreported miRNAs (miRNA-203, miRNA-369-5p, miRNA-376a, and miRNA-375) whose expression is significantly different in PDAC rats compared to control rats. These miRNAs need to be quantitated in humans as potential novel clinical diagnostic biomarkers for PDAC.

Key Words: pancreatic cancer, animal model, transgenic rat, circulating miRNA, biomarker

(*Pancreas* 2012;41: 1013–1018)

Pancreatic cancer is diagnosed in approximately 1 person per 10,000 annually in the United States and is the fifth leading cause of cancer death. Most patients die within 1 year of diagnosis, and the 5-year survival rate is less than 5%.[1] Pancreatic ductal adenocarcinomas (PDACs) are diagnosed in 95% of the patients with pancreatic cancer. The most widely used marker for pancreatic cancer, CA19-9, is unfortunately also elevated in cases of benign cholangitis, pancreatitis, and other cancers and therefore lacks specificity for detecting potentially curable lesions.[2–4] Consequently, there is presently no valid approach for early detection of pancreatic cancer, and therefore, there is an urgent need for new and more specific and sensitive biomarkers for pancreatic cancer.

MicroRNAs (miRNAs) are evolutionarily conserved 18 to 24 nucleotide RNA molecules that regulate the stability and translational efficiency of target mRNAs by complementary base pairing with specific 3′ untranslated region sequences.[5] Such physiologic regulation of transcriptome function by miRNAs plays a significant role in regulating diverse biological processes such as cell proliferation, differentiation, tissue development, and cell death.[6] Aberrant expression of miRNAs in lesions has been widely reported in diseases and tumors, including pancreatic cancers.[7–13] Recently, several studies have shown that circulating miRNAs can be detected in plasma/serum; the mechanisms by which these miRNAs are protected from endogenous RNase activity is unknown.[14] Some studies have indicated that fluctuation of specific circulating miRNAs reflects various physiological changes, diseases, and cancers.[15–17] Recently, elevation of miR-21, miR-210, miR-155, and miR-196a in the plasma of patients with PDAC was reported.[18] These findings point to the possibility that circulating miRNAs could be novel biomarkers for the diagnosis of PDAC. Plasma/serum samples are attractive for biomarker assays because their procurement involves minimal invasion.

Previously, we established transgenic rats in which expression of the human H-*ras*^{G12V} or K-*ras*^{G12V} oncogene is regulated by the *Cre/lox* system.[19–21] Targeted activation of H-*ras*^{G12V} or K-*ras*^{G12V} is accomplished by injection of a *Cre*-carrying adenovirus into the pancreatic ducts and acini through the common bile duct. H-*ras* or K-*ras* transgenic rats develop identical PDACs: Several weeks after injection, proliferative lesions in the duct epithelium, intercalated ducts, and centroacinar cells, but not acinar cells, become widespread. The histopathological appearance of these adenocarcinomas closely resembles that described for typical pancreatic tumors in man. Thus, these transgenic rats with inducible PDACs (PDAC rats) are a rat model for human PDAC. In this study, human K-*ras* transgenic rats were used because K-*ras* oncogene mutations are commonly observed in human PDAC.

Genetically engineered model animals afford defined stages of tumor development, homogenized breeding, control of environmental conditions, and standardized blood sampling, thereby reducing biological and nonbiological heterogeneity. Therefore, discovery of novel biomarkers using suitable animal models for human PDAC is much more practical than using human samples.

In this study, we compared the amounts of circulating miRNAs in the serum of PDAC rats with those of rats with a normal pancreas (control rats) to find novel candidate clinical diagnostic biomarkers for PDAC. The miRNAs, which were quantified, were identified using microarray analysis of serum and pancreatic tissues of control and PDAC rats. Our findings add to the list of miRNAs previously reported to be high in patients with PDAC.

From the *Toxicology Group, Environmental Health Science Laboratory, Sumitomo Chemical Co, Ltd, Osaka, Japan; Departments of †Molecular Toxicology, and ‡Gastroenterology and Metabolism, Nagoya City University Graduate School of Medical Sciences; and §Nanotoxicology Project, Nagoya City University, Nagoya, Japan.

Received for publication September 14, 2011; accepted January 10, 2012.

Reprints: Setsuko Yabushita, MS, Toxicology Group, Environmental Health Science Laboratory, Sumitomo Chemical Co, Ltd, 1-98, 3-chome, Kasugade-naka, Konohana-ku, Osaka 554-8558, Japan (e-mail: yabushitas@sc.sumitomo-chem.co.jp).

The authors declare no conflict of interest.

MATERIALS AND METHODS

Induction of Pancreatic Ductal Adenocarcinomas

The generation of Kras301 rats carrying the K-*ras*^{G12V} transgene has been described previously.[19–21] Adenovirus vector carrying the *Cre* gene (AxCANCre) and empty adenovirus vector (AxCAwt) were injected into the pancreatic ducts of 10- to 11-week-old adult homozygous male Kras301 rats through the common duct as previously reported.[19] Six rats were treated with AxCANCre (PDAC rats) and 4 rats were treated with AxCAwt (control rats). Rats were maintained in cages in an air-conditioned room with a 12-hour light/12-hour dark cycle. Rats were euthanized by blood withdrawal from the abdominal aorta under anesthesia 16 to 17 days after the injection of adenovirus vector: these animals exhibited advanced PDAC development. The experiments were conducted in accordance with the "Guidelines for Animal Experiments of the Nagoya City University Graduate School of Medical Sciences."

Pathological Examination

Pancreases were excised from autopsied rats, and tumor containing tissue from PDAC rats and normal pancreas tissue from control rats was immediately frozen in liquid nitrogen. The remaining pancreas tissues were fixed in 4% paraformaldehyde, processed for embedding in paraffin, cut into sections about 3 μm in thickness, and stained with hematoxylin and eosin for microscopic examination.

RNA Extraction from Pancreatic Tissues and Serum

Total RNA was isolated from frozen pancreatic tumors of PDAC rats and pancreatic tissues of control rats by using ISOGEN (Nippon Gene, Toyama, Japan) in accordance with the manufacturer's instructions. Total RNA extracted from normal pancreatic tissues was resuspended in RNAsecure reagent (Applied Biosystems, Tokyo, Japan) for protection against degradation.

Total RNA was isolated from 4 mL of serum for microarray analysis and 0.48 mL of serum for real-time quantitative reverse transcription polymerase chain reaction (qRT-PCR) using mirVana PARIS Kit (Applied Biosystems), in accordance with the manufacturer's instructions with the following minor modification: The serum for microarray analysis was mixed with an equal volume of acid-phenol chloroform and centrifuged 3 times because of the presence of abundant proteins. A 0.24-mL portion of the serum for qRT-PCR was spiked with 0.2 fmol of synthetic miR-3 from *Drosophila melanogaster* (dme-miR-3) as an internal standard after denaturing the serum. Total RNA for qRT-PCR was extracted from serum twice, using 0.48 mL serum in total, and pooled for each animal.

MicroRNA Microarray Analysis

MicroRNA microarray analysis was conducted on total RNA samples extracted from pancreatic tissues and serum by using a rat miRNA microarray kit (Agilent Technologies, Santa Clara, Calif) that had probes for 350 rat miRNAs. The procedure was conducted following the manufacturer's instructions (version 2.0), and Feature Extraction (version 10.5) was used to generate a quantitative signal value and a qualitative detection call for each probe on the microarray (Agilent Technologies). A 75th percentile normalization was used for per-sample normalization. Normalized miRNA expression data were analyzed with Welch's *t* test to obtain miRNAs that were significantly altered in comparison with expression in control samples at a probability level of 5% by 2-sided Welch *t* tests. The serum miRNAs were applied to unsupervised and supervised hierarchical clustering analyses with GeneSpring GX 7.3.1 (Agilent Technologies). Pearson and standard correlations were used for similarity measurement of genes and samples, respectively.

Real-Time Quantitative RT-PCR of Mature miRNAs

Quantitative RT-PCR of mature miRNAs was conducted using the same RNA samples as were used for microarray analysis. Quantification was performed using TaqMan MicroRNA assays and 7500 Fast Real-Time PCR Systems (Applied Biosystems) in accordance with the manufacturer's instructions with the following minor modifications: Some PCR reaction mixtures included the RT reaction product diluted at a ratio of 1:4. The experiment was conducted in duplicate. The cycle threshold (Ct) was determined using the Ct of internal controls, U6 in pancreatic tissues, or spiked dme-miR-3 in serum. The relative intensity of miRNA expression was represented by $2^{-\Delta Ct}$, in which ΔCt was generated by deducing the Ct of U6 or dme-miR-3 from the Ct of each miRNA. All primers used were purchased from Applied Biosystems. For analysis of the relative intensity, *F* test in ARM EXSUS version 7.6 (Arm Systex Co Ltd, Osaka, Japan) was applied to test the homogeneity of variance between the control and the PDAC rats. If homogeneous, the data were analyzed with Student *t* test, and if not, with Welch *t* test. Significance of differences from the control rats were estimated at a probability level of 5% by one-sided Student or Welch *t* tests for the relative levels of miRNAs in the serum and 2-sided Student or Welch *t* tests for the relative levels of miRNAs in pancreatic tissues. In addition to statistical evaluation, serum miRNAs whose levels were not statistically higher than that of the control but for which the levels of 4 or more PDAC rats were higher than the highest level of the control rats were also regarded to be higher than control.

RESULTS AND DISCUSSION

Pathological Observation

Kras301 rats, 13 to 14 weeks of age, were killed 16 to 17 days after injection of adenovirus vector into the pancreatic duct via the common bile duct. Gross and histological findings were the same as reported previously[19]: PDAC was well developed with grossly visible whitish lesions in all of the 6 rats treated with AxCANCre. Histopathological examination showed that the lesions were adenocarcinomas with a variable amount of fibrotic tissue proliferation, some showing desmoplastic morphology and infiltration of inflammatory cells. Neoplastic lesions were not grossly visible in any other organs. By gross observation and histopathological examination, no abnormalities were observed in the pancreatic tissues of the 4 rats injected with AxCAwt.

Grossly visible tumors in PDAC rats can also be detected by ultrasound[21]; therefore, these tumors are roughly at a similar stage as those in human patients when PDAC is initially detected. The primary difference between the PDAC rat and a human PDAC patient is that the PDAC are not metastatic in our animal model.

Quantitative RT-PCR of Mature miRNAs in Serum, Previously Reported to be Increased in the Plasma of Patients With PDAC

Four serum miRNAs (miR-210, miR-21, miR-155, and miR-196a) reported to be high in the plasma of patients with PDAC were quantified by qRT-PCR. The results are shown in Table 1 (A). In contrast to the levels in patients with PDAC, only miR-155 was significantly elevated (Fig. 1): miR-21 and miR-210 were nonsignificantly elevated and miR-196a was not changed. Overall, 3 of these 4 miRNAs tended to be increased in PDAC

TABLE 1. Serum miRNAs Quantified by qRT-PCR and Their Expression in the Serum and Pancreatic Tissues of Control Rats and PDAC Rats

	Serum†					Pancreas‡				
	Relative Intensity		Fold		PDAC	Relative Intensity		Fold		PDAC
microRNA	Control	PDAC	Change	*P*	Patients§	Control	PDAC	Change	*P*	Patients§
(A) Serum miRNAs selected for quantification based on a previous report of increased plasma miRNAs in PDAC patients										
miR-210	0.48	0.84	1.7 ↑	0.075	↑[18]	0.68	0.69	1.0	0.959	↑[8–10]
miR-21	5.25	7.98	1.5 ↑	0.062	↑[18]	28.24	453.46	16.1 ↑*	0.000	↑[7,8]
miR-155	0.08	0.11	1.5 ↑*	0.002	↑[18]	0.02‖	0.05‖	2.9 ↑*	0.036	↑[7–10,12]
miR-196a	0.0021	0.0023	1.1	0.334	↑[18]	−0.19	−0.03		0.094	↑[9–11]
(B) Serum miRNAs selected for quantification based on results of miRNA microarray analysis of serum in control and PDAC rats										
Up-regulated miRNAs¶										
miR-30b-5p	6.48	9.34	1.4 ↑	0.095		8.74	5.46	0.6	0.074	
miR-24-2*	0.68	0.93	1.4	0.213		−0.33	0.34	↑*	0.000	
miR-20b-5p	0.81	1.10	1.4	0.216		0.57	−0.04		0.564	
miR-874	0.007	0.008	1.2	0.181		0.73	0.05	0.1	0.218	
miR-125b-3p	0.00034	0.00027	0.8	0.246		−0.31	−0.04		0.020	
miR-125b*	0.006	0.005	0.1	0.325		0.95	0.29	0.3 ↓*	0.003	
Down-regulated miRNAs#										
let-7c	0.72	1.05	1.5	0.143		45.00	24.57	0.5 ↓*	0.030	
let-7b	0.92	1.30	1.4	0.153		40.04	17.72	0.4 ↓*	0.007	
miR-125a-5p	0.02	0.024	1.2	0.301		1.01	1.58	1.6 ↑*	0.018	↑[8]
miR-375	0.16	0.11	0.7 ↓*	0.027		12.42	−0.01	↓*	0.002	↓[8–10]
(C) Serum miRNAs selected for quantification based on results of miRNA microarray analysis of pancreatic tissues in control and PDAC rats										
Up-regulated miRNAs**										
miR-541	5.00E-05	0.0029	63.2 ↑	0.069		−0.29	0.02	↑*	0.012	
						0.0005‖	0.0039‖	7.1 ↑*	0.019	
miR-369-5p	1.00E-05	0.0001	12.2 ↑*	0.046		−0.09	0.06	↑*	0.011	
						0.0002‖	0.0010‖	5.9 ↑*	0.020	
miR-376a	0.002	0.017	7.4 ↑*	0.046		−0.26	0.18	↑*	0.002	↑[7]
miR-31	0.043	0.129	3.0 ↑	0.068		0.80	4.95	6.2 ↑*	0.000	↑[9,10]
miR-93	3.80	6.21	1.6	0.123		0.07	1.05	15.0 ↑*	0.000	↑[10]
miR-18a	3.38	5.50	1.6 ↑	0.069		−0.26	0.31	↑*	0.002	
miR-301a	1.25	1.99	1.6	0.130		0.09	1.26	14.0 ↑*	0.000	↑[7]
miR-542-3p	0.007	0.009	1.4	0.216		−0.19	0.47	↑*	0.001	
miR-203	0.158	0.205	1.3 ↑*	0.021		0.16	0.86	5.3 ↑*	0.011	↑[10,12,13]
miR-145	2.63	3.00	1.1	0.418		0.41	0.91	2.2 ↑*	0.030	↑[9,10]
miR-205	0.018	0.019	1.0	0.468		−0.10	0.45	↑*	0.003	↑[8–10]
miR-224	0.0003	0.0003	0.9	0.411		−0.23	0.01	↑*	0.013	↑[10]
miR-222	0.433	0.265	0.6	0.099		−0.17	1.17	↑*	0.000	↑[8,10–12]
miR-16	111.13	45.41	0.4	0.143		13.14	43.04	3.3 ↑*	0.002	↑[7]
Down-regulated miRNAs††										
miR-29c	4.79	6.58	1.4	0.135		8.62	3.22	0.4 ↓*	0.027	↓[10]
miR-141	0.012	0.013	1.1	0.212		20.37	3.63	0.2 ↓*	0.004	↓[10]
miR-217	2.70E-05	2.60E-05	1.0	0.474		1.10	−0.07	↓*	0.009	↓[9,10]
miR-216a	0.00028	0.00014	0.5	0.133		20.13	−0.07	↓*	0.007	↓[10]

Fold change was calculated from the relative intensities of control and PDAC rats.

*Statistical significance ($P < 0.05$).

†MiRNAs in the serum of 4 control and 6 PDAC rats were quantified by qRT-PCR.

‡MiRNAs in pancreatic tissues of 4 control and 4 PDAC rats were quantified by miRNA microarray analysis.

§Up- and down-regulation reported in PDAC patients.

‖MiRNAs in pancreatic tissue of 4 control and 4 PDAC rats were quantified by qRT-PCR.

¶Up-regulated miRNAs in the serum of PDAC rats as indicated by miRNA microarray analysis of serum in 3 control rats and 3 PDAC rats.

#Down-regulated miRNAs in the serum of PDAC rats as indicated by miRNA microarray analysis of serum in 3 control and 3 PDAC rats.

**Up-regulated miRNAs in pancreatic tumor tissue of PDAC rats as indicated by miRNA microarray analysis of normal and tumor pancreatic tissue in 4 control and 4 PDAC rats.

††Down-regulated miRNAs in pancreatic tumor tissue of PDAC rats as indicated by miRNA microarray analysis of normal and tumor pancreatic tissue in 4 control and 4 PDAC rats.

↑Up-regulated; ↓ down-regulated.

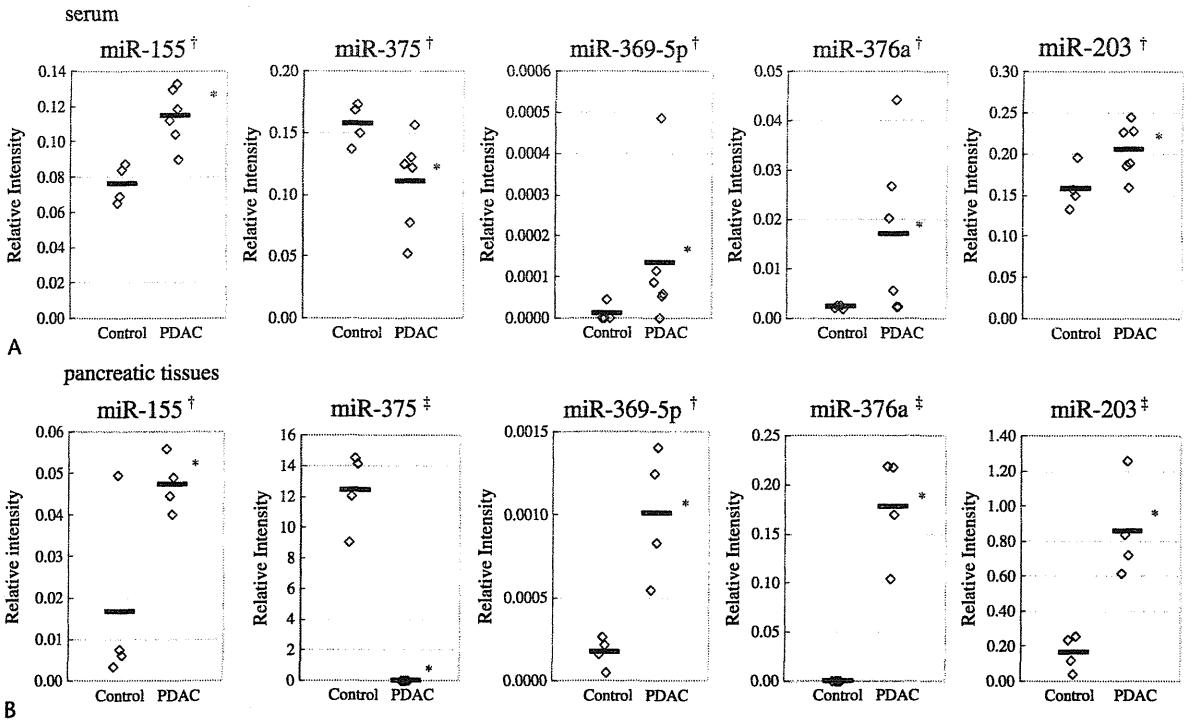

FIGURE 1. Change in the expression of mature miRNAs in the serum of control rats and PDAC rats. The finding that miR-375, miR-369-5p, miR-376a, and miR-203 are differentially expressed in the serum of PDAC rats is new. MiR-155, which is known to be high in plasma of patients with PDAC, was also elevated in the rat model. *Significant with $P < 0.05$; †data of qRT-PCR; ‡data of microarray.

rats compared to the control rats. Therefore, these results suggest that using this rat model to find novel circulating diagnostic biomarkers for patients with PDAC is feasible. Consequently, miRNA microarray analyses of serum and pancreatic tissues were performed to screen for novel candidate biomarkers of PDAC.

MicroRNA Microarray Analysis of Serum

Total RNA extracted from the sera of 3 control and 3 PDAC rats was subjected to miRNA microarray analysis. Unsupervised hierarchical clustering using all miRNA expression values clearly separated the PDAC rats from the control rats (Fig. 2A), which demonstrates the potential of using serum miRNAs as biomarkers of PDAC. Therefore, we carried out a supervised hierarchical clustering analysis to identify specific serum miRNAs that can differentiate the PDAC rats from the control rats. To perform this supervised hierarchical clustering analysis, 15 serum miRNAs were selected based on their statistical significance ($P < 0.05$) from control. Fold changes of the selected miRNAs were from 1.3 to 14.4 (miR-30b-5p, miR-24-2*, miR-20b-5p, miR-874, miR-125b-3p, miR-125b*, miR-29a, miR-365, miR-370, and miR-878) and from 0.2 to 0.6 (let-7c, let-7b, miR-125a-5p, miR-375, and miR-466b). This supervised hierarchical clustering provided clear clusters to differentiate the control rats from the PDAC rats (Fig. 2B).

Quantitative RT-PCR of Mature miRNAs in Serum Selected by Microarray Analyses of Serum

Among 15 serum miRNAs for which differences between the PDAC rats and the control rats were found by miRNA microarray analysis, 10 serum miRNAs (miR-30b-5p, miR-24-2*, miR-20b-5p, miR-874, miR-125b-3p, miR-125b*, let-7c, let-7b, miR-125a-5p and miR-375) were selected for quantification by qRT-PCR (Table 1 [B]), and 5 miRNAs were excluded: miR-466b and miR-878 are not expressed in humans; MiR-29a and miR-365 are reported to be overexpressed in the plasma of a rodent model of liver injury; and miR-29a and miR-370 are reported to be suppressed in rodent models of liver damage.[16,22] MicroRNAs, which varied in models of tissue damage, were excluded to limit the likelihood of identifying miRNAs, which varied because of nontumor events, for example, inflammation. Among the 10 serum miRNAs quantified by qRT-PCR, there was a significant decrease of miR-375 (Fig. 1) and a nonsignificant increase of miR-30b-5p. The other miRNAs were the same in the PDAC rats and the control rats. Causes of the discrepancy between the miRNA microarray and qRT-PCR results are uncertain but are likely due to the low quantitative precision of the microarray analysis. The finding that miRNA-375 is significantly decreased in the serum is new.

MicroRNA Microarray Analysis of Pancreatic Tissues

Total RNA extracted from the pancreatic tissues of 4 control rats and pancreatic tumor tissues of 4 PDAC rats were subjected to miRNA microarray analysis. Numerous miRNAs showed different expression levels between the control rats and the PDAC rats (data not shown). miR-541, miR369-5p, and miR-155 in the pancreatic tissues of the control rats and the PDAC rats were quantified by qRT-PCR. The relative intensity of miR-155 was not analyzed by the microarray analysis because of the lack of a relevant probe for miR-155. MiR-541 and miR-369-5p levels

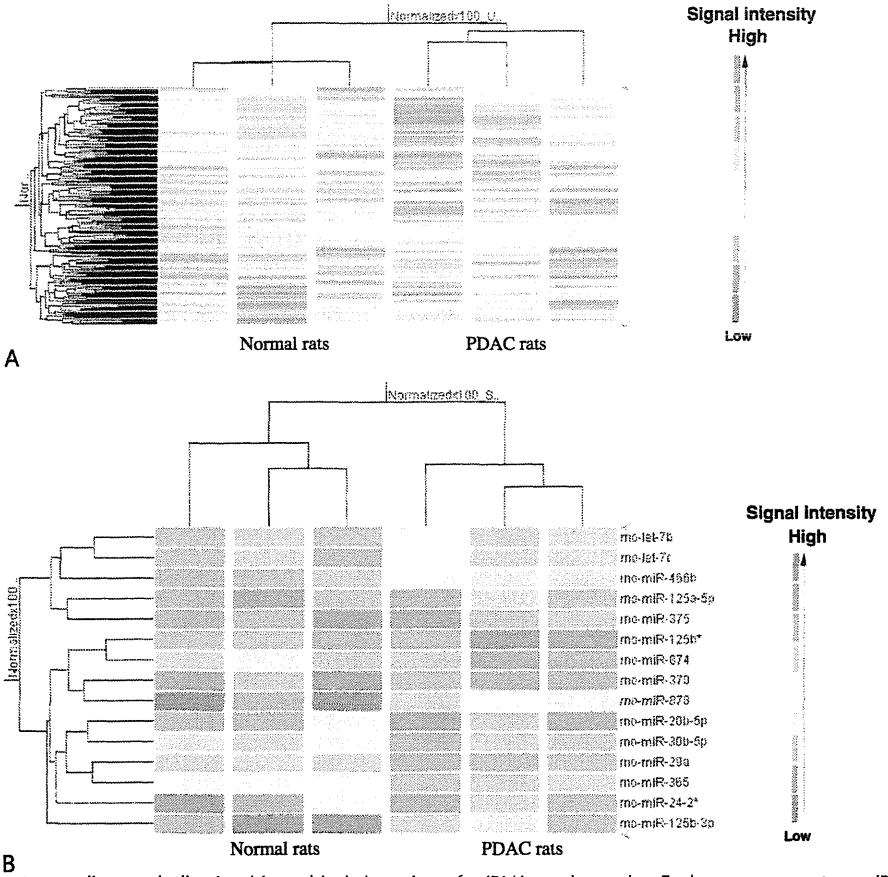

FIGURE 2. The heat map diagram indicating hierarchical clustering of miRNAs and samples. Each row represents a miRNA, and each column represents a sample. The miRNA clustering tree is shown on the left, and the sample clustering tree appears at the top. The color scale shown on the right illustrates the relative expression level of the miRNA. A clustering dendrogram shows differential expression profiles of circulating miRNAs in the sera of normal rats and PDAC rats. A, Unsupervised hierarchical clustering. B, Supervised hierarchical clustering.

detected by microarray were very low; therefore, we confirmed the microarray data by qRT-PCR. The microarray and qRT-PCR data were consistent with each other.

Quantitative RT-PCR of Mature miRNAs in Serum Selected by Microarray Analyses of Pancreatic Tissues

Among the variety of miRNAs for which differences between the PDAC rats and the control rats were found by miRNA microarray analysis, 18 serum miRNAs were quantified by qRT-PCR (Table 1 [C]). All of these miRNAs are known to exist in humans. Among the 14 miRNAs overexpressed in pancreatic tumor tissues of the PDAC rats, miR-369-5p, miR-376a, and miR-203 were significantly increased (Fig. 1); and miR-541, miR-31, and miR-18a were nonsignificantly increased in the serum of the PDAC rats. None of the miRNAs with reduced expression in the pancreatic tumor tissues of PDAC rats was altered in the serum of the PDAC rats. Thus, among these 18 serum miRNAs, qRT-PCR revealed 6 miRNAs, which were altered, 3 significantly, in the serum of the PDAC rats. The finding that miRNA-369-5p, miRNA-376a, and miRNA-203 are significantly increased in the serum is new.

These results demonstrate that miRNA microarray analysis of pancreatic tissues enables discovery of candidate circulating miRNAs as biomarkers of PDACs. Surprisingly, miRNA microarray analysis of PDAC was more effective than miRNA microarray analysis of the serum in identifying serum-miRNA markers of PDAC, although the efficiency of miRNA microarray analysis of serum might be increased by technical improvements in the future.

Aberrantly Expressed miRNAs in the Serum of PDAC Rats

Among the aberrantly expressed miRNAs in the serum of the PDAC rats, miR-155, miR-375, miR-369-5p, miR-376a, and miR-203 likely arose from the pancreatic lesions, as similar changes were observed in pancreatic tumor tissues. Furthermore, among these 5 miRNAs, changes of miR-155, miR-375, miR-376a, and miR-203 in pancreatic tumor tissues of the PDAC rats were consistent with those of the patients with PDAC.[7–10,12] The increase in miRNA-369-5p is a new finding. Aberrantly expressed miRNAs are known to be related to tumorigenesis[23]: miR-155 is known to repress tumor protein 53–induced nuclear protein, which enhances tumor development of pancreatic cancer cells in vivo,[24] and overexpression of miR-203 is correlated with a poorer survival in patients with pancreatic and colon adenocarcinomas.[12,25]

Circulating miR-155 and miR-203 have also been reported to be overexpressed in patients with cancers other than PDAC: miR-155 in diffuse large B-cell lymphoma and miR-203 in ovarian cancers.[26] Therefore, these circulating miRNAs are not specific to PDAC. However, such cancer biomarkers might constitute PDAC-specific markers if combined in a panel with pancreas-specific ones such as miR-375, which is known to be expressed specifically in pancreatic islets.[27] Currently, although there are no reports about circulating miR-375 in patients with PDAC, it may decrease because miR-375 is reported to decrease in pancreatic tumor tissues of patients with PDAC[8–10]; and it was found to be decreased in both serum and pancreatic tumor tissues of the PDAC rats in the present study.

In conclusion, some differentially expressed miRNAs (miRNA-155, miRNA-375, miRNA-369-5p, miRNA-376a, and miRNA-203) were identified in the serum of PDAC rats. MiRNA-155 has already been reported to be elevated in the plasma of patients with PDAC; the finding that miRNA-375, miRNA-369-5p, miRNA-376a, and miRNA-203 are differentially expressed in the serum is new. The results indicate that use of our rat model for human PDAC to find novel candidate circulating miRNAs as biomarkers for human PDAC is feasible. The differentially expressed serum miRNAs identified in this model are potential clinical diagnostic biomarkers for PDAC and need to be examined in the blood of human patients with PDAC.

ACKNOWLEDGMENTS

The authors thank Keiko Tanaka of Environmental Health Science Laboratory, Sumitomo Chemical Co, Ltd for technical assistance. The authors also thank Dr David Alexander of the Nanotoxicology Project, Nagoya City University, for critical reading of the manuscript.

REFERENCES

1. Jemal A, Murray T, Samuels A, et al. Cancer statistics, 2003. *CA Cancer J Clin.* 2003;53:5–26.
2. Akdogan M, Sasmaz N, Kayhan B, et al. Extraordinarily elevated CA19-9 in benign conditions: a case report and review of the literature. *Tumori.* 2001;87:337–339.
3. Ni XG, Bai XF, Mao YL, et al. The clinical value of serum CEA, CA19-9, and CA242 in the diagnosis and prognosis of pancreatic cancer. *Eur J Surg Oncol.* 2005;31:164–169.
4. Duffy MJ. CA 19-9 as a marker for gastrointestinal cancers: a review. *Ann Clin Biochem.* 1998;35:364–370.
5. Chang TC, Mendell JT. MicroRNAS in vertebrate physiology and human disease. *Annu Rev Genomics Hum Genet.* 2007;8:215–239.
6. Ambros V. The functions of animal microRNAs. *Nature.* 2004;431:350–355.
7. Lee EJ, Gusev Y, Jiang J, et al. Expression profiling identifies microRNA signature in pancreatic cancer. *Int J Cancer.* 2007;120:1046–1054.
8. Bloomston M, Frankel WL, Petrocca F, et al. MicroRNA expression patterns to differentiate pancreatic adenocarcinoma from normal pancreas and chronic pancreatitis. *J Am Med Assoc.* 2007;297:1901–1908.
9. Szafranska AE, Doleshal M, Edmunds HS, et al. Analysis of microRNAs in pancreatic fine-needle aspirates can classify benign and malignant tissues. *Clin Chem.* 2008;54:1716–1724.
10. Szafranska AE, Davison TS, John J, et al. MicroRNA expression alterations are linked to tumorigenesis and non-neoplastic processes in pancreatic ductal adenocarcinoma. *Oncogene.* 2007;26:4442–4452.
11. Zhang Y, Li M, Wang H, et al. Profiling of 95 microRNAs in pancreatic cancer cell lines and surgical specimens by real-time PCR analysis. *World J Surg.* 2009;33:698–709.
12. Greither T, Grochola LF, Udelnow A, et al. Elevated expression of microRNAs 155, 203, 210 and 222 in pancreatic tumors is associated with poorer survival. *Int J Cancer.* 2010;126:73–80.
13. Ikenaga N, Ohuchida K, Mizumoto K, et al. MicroRNA-203 expression as a new prognostic marker of pancreatic adenocarcinoma. *Ann Surg Oncol.* 2010;17:3120–3128.
14. Tsui NB, Ng EK, Lo YM. Stability of endogenous and added RNA in blood specimens, serum, and plasma. *Clin Chem.* 2002;48:1647–1653.
15. Gilad S, Meiri E, Yogev Y, et al. Serum microRNAs are promising novel biomarkers. *PLoS One.* 2008;3:e3148.
16. Wang K, Zhang S, Marzolf B, et al. Circulating microRNAs, potential biomarkers for drug-induced liver injury. *Proc Natl Acad Sci U S A.* 2009;106:4402–4407.
17. Mitchell PS, Parkin RK, Kroh EM, et al. Circulating microRNAs as stable blood-based markers for cancer detection. *Proc Natl Acad Sci U S A.* 2008;105:10513–10518.
18. Wang J, Chen J, Chang P, et al. MicroRNAs in plasma of pancreatic ductal adenocarcinoma patients as novel blood-based biomarkers of disease. *Cancer Prevention Research (Philadelphia, PA).* 2009;2:807–813.
19. Ueda S, Fukamachi K, Matsuoka Y, et al. Ductal origin of pancreatic adenocarcinomas induced by conditional activation of a human Ha-*ras* oncogene in rat pancreas. *Carcinogenesis.* 2006;27:2497–2510.
20. Tanaka H, Fukamachi K, Futakuchi M, et al. Mature acinar cells are refractory to carcinoma development by targeted activation of ras oncogene in adult rats. *Cancer Sci.* 2010;101:341–346.
21. Fukamachi K, Tanaka H, Hagiwara Y, et al. An animal model of preclinical diagnosis of pancreatic ductal adenocarcinomas. *Biochem Biophys Res Commun.* 2009;390:636–641.
22. Fukushima T, Hamada Y, Yamada H, et al. Changes of micro-RNA expression in rat liver treated by acetaminophen or carbon tetrachloride—regulating role of micro-RNA for RNA expression. *J Toxicol Sci.* 2007;32:401–409.
23. Davis-Dusenbery BN, Hata A. MicroRNA in cancer: the involvement of aberrant microRNA biogenesis regulatory pathways. *Genes and Cancer.* 2010;1:1100–1114.
24. Gironella M, Seux M, Xie MJ, et al. Tumor protein 53-induced nuclear protein 1 expression is repressed by mir-155, and its restoration inhibits pancreatic tumor development. *Proc Natl Acad Sci U S A.* 2007;104:16170–16175.
25. Schetter AJ, Leung SY, Sohn JJ, et al. MicroRNA expression profiles associated with prognosis and therapeutic outcome in colon adenocarcinoma. *JAMA.* 2008;299:425–436.
26. Taylor DD, Gercel-Taylor C. MicroRNA signatures of tumor-derived exosomes as diagnostic biomarkers of ovarian cancer. *Gynecol Oncol.* 2008;110:13–21.
27. Poy MN, Eliasson L, Krutzfeldt J, et al. A pancreatic islet-specific microRNA regulates insulin secretion. *Nature.* 2004;432:226–230.

BUNSEKI KAGAKU Vol. 61, No. 9, pp. 783–790 (2012)

報　文

キラル高速液体クロマトグラフィー/大気圧化学イオン化質量分析法によるグリシドール脂肪酸エステルの光学異性体分析

吉岡　智史[1]，西村　一彦[2]，高村　岳樹[3]，酒々井眞澄[4]，津田　洋幸[4]，板橋　豊[5]

キラル高速液体クロマトグラフィー/質量分析法（HPLC/MS）を用いて，食用油に微量存在し，安全性が危惧されているグリシドール脂肪酸エステル（GE）の光学異性体を分離，定量する方法を検討した．HPLC分析には，アミロース誘導体を固定相とするカラムとアセトニトリルに少量のメタノールを添加した移動相を使用した．MSには四重極型質量分析計を用いて，大気圧化学イオン化法で正イオンスペクトルを測定した．その結果，炭素数と不飽和度の異なるGEの光学異性体が明瞭に分離され，それぞれから顕著なプロトン化分子 $[M+H]^+$ が検出された．このイオンを用いる選択イオン検出法によって，ジアシルグリセロールを約80 % 含有する食用油（DAG油）を直接分析した結果，アシル基の異なる5種のGE（16 : 0-GE，18 : 0-GE，18 : 1-GE，18 : 2-GE，18 : 3-GE）が検出され，これらはいずれも（*R*)-異性体と（*S*)-異性体のほぼ等量混合物であることが明らかになった．得られた結果から，DAG油に含まれるGEの光学異性体は，ほぼラセミ体の1-モノアシルグリセロールから生成するものと考えられた．

1　緒　　言

食用油（精製植物油）に微量含まれるグリシドール脂肪酸エステル（GE，1-アシル-2,3-エポキシプロパン）の安全性が危惧されており，世界的に大きな問題となっている[1)2)]．GEは，食用油の主成分であるトリアシルグリセロール（TAG）やジアシルグリセロール（DAG）が脱臭などの精製工程で高温，高圧下に置かれることで生成すると考えられている[2)3)]．

食用油に含まれる微量のGEを精確に定量することは容易ではなく，信頼のおける分析法の開発が緊急の課題となっている[1)]．これまで，GEの分析法がいくつか報告されている．たとえば，Masukawa[4)5)]らは食用油中のGEを2回の固相抽出によって濃縮した後，逆相高速液体クロマトグラフィー/質量分析法（HPLC/MS）を用いてアシル基の異なる5種のGEを定量している．Weißhaar[3)]らは食用油中のGEをゲル沪過によって分離後，ガスクロマトグラフィー/質量分析法（GC/MS）を用いて同定している．一方，Deutsche Gesellschaft für Fettwissenschaft（DGF，ドイツ脂質科学会）[6)]は，GEを加水分解して生成する3-モノクロロ-1,2-プロパンジオールをフェニルホウ酸で誘導体化した後，GC/MSを用いてGEを間接的に定量する方法を推奨している．これらの方法は，食用油に含まれるGEの検出と定量に有用であると思われるが，存在可能な1対の光学異性体（Fig. 4参照）については何も考慮されていない．GEの光学異性体間の生物活性の差異は明らかではないが，光学異性体は，一方が有効な活性を示し，もう一方が毒性を示すなど生物に対する作用が異なる場合があることから，食品中のGEをリスク評価する際には，安全性が危惧されているGEの光学異性体分析は不可欠であると考えられる．

本研究では逆相キラルHPLCを用いてGEの光学異性体を分離し，MSを併用して前処理なしで実試料中のGE光学異性体を直接分析する方法を検討した．得られた結果からGE光学異性体の生成経路を推測した．

2　実　　験

2·1　試　薬

以下の試薬を用いた．パルミチン酸（16 : 0），ステアリン酸（18 : 0），オレイン酸（18 : 1），リノール酸（18 : 2），リノレン酸（18 : 3）（Sigma製，純度99 % 以上）；パルミチン酸グリシジル（16 : 0-GE，純度98 % 以上），オレイン酸グリシジル（18 : 1-GE，純度98 % 以上），リノール酸グ

✉ E-mail : yutaka@fish.hokudai.ac.jp
[1] 北海道大学大学院水産科学院海洋応用生命科学分野：041-8611 北海道函館市港町 3-1-1
[2] 北海道立衛生研究所：060-0819　北海道札幌市北区北19条西12丁目
[3] 神奈川工科大学工学部応用化学科：243-0292　神奈川県厚木市下荻野 1030
[4] 名古屋市立大学大学院医学研究科分子毒性学分野：467-8601 愛知県名古屋市瑞穂区瑞穂町字川澄 1
[5] 北海道大学大学院水産科学研究院海洋応用生命科学部門：041-8611　北海道函館市港町 3-1-1

リシジル（18 : 2-GE，純度 90 % 以上），リノレン酸グリシジル（18 : 3-GE，純度 85 % 以上）（和光純薬工業製）；4-ジメチルアミノピリジン（DMAP），無水硫酸ナトリウム，*N*,*N*-ジシクロヘキシルカルボジイミド（DCC）（ナカライテスク製）；(*R*)-，(*S*)-及びラセミ体グリシドール（Aldrich 製，純度 96～97 %）；DAG 高含有（約 80 %）食用油[7]（DAG 油，花王製，2008 年に函館市内の食料品店にて購入）．

2・2 GE 標準品の合成

(*R*)-グリシドール，(*S*)-グリシドール及びラセミ体グリシドール（各 0.9 mmol），脂肪酸（1.0 mmol），DCC（1.2 mmol），DMAP（0.2 mmol）をクロロホルム 5 mL に溶解し，撹拌しながら 20 ℃ で 16 時間反応させた．沪過後，クロロホルムを窒素気流下で除去して得られた残渣約 20 mg を 200 μL のクロロホルムに再度溶解させた．このクロロホルム可溶物からシリカゲル薄層クロマトグラフィー｛Merck 製シリカゲル 60 F_{254}（厚さ 0.25 mm, 20 cm × 20 cm)｝を用いて GE を単離した．展開溶媒にはヘキサン-ジエチルエーテル（60 : 40, v/v）を使用した．展開後，0.2 % 2',7'-ジクロロフルオレセイン試薬を噴霧して，紫外線照射下で市販標準品と同一の R_f 値を示すバンドを確認し，ジエチルエーテルを用いて抽出した．得られた GE 画分を大気圧化学イオン化質量分析法（APCI-MS）で確認し，その純度を光散乱検出逆相 HPLC（HPLC/ELSD）で求めた．MS には四重極型質量分析計 LC/MS-2010EV（島津製作所製）を用い，インフュージョン法で GE のマススペクトルを m/z 200～m/z 1000 の範囲で測定した．ネブライザーガス 2.5 L min^{-1}，インターフェース温度 400 ℃，加熱ブロック温度 200 ℃ に設定し，正イオンスペクトル測定した．HPLC 分析には Gemini 5u C18 110A カラム（Penomenex 製，内径 4.6 mm，長さ 25 cm，粒径 5 μm），LC-20AD ポンプ（島津製作所製），カラム恒温槽 Cool Pocket（Thermo Fisher Scientific 製），蒸発光散乱検出器（SEDEX55，SEDERE 製）及びクロマトパック C-R6A（島津製作所製）を使用した．試料は 2-プロパノールに 1 mg mL^{-1} の濃度になるように溶解し，その 5 μL を Rheodyne 製インジェクター（Model 7725）を用いてカラムに注入した．移動相にはアセトニトリル/メタノール（10 : 90, v/v）（関東化学製 HPLC 用）を用いて 0.5 mL min^{-1} の流量で送液した．カラム温度は 20 ℃ とし，検出器の温度を 50 ℃（空気圧力 2.3 bar，Gain 8）に設定して溶出成分を検出した．

2・3 キラル HPLC/ELSD 分析

キラル HPLC 分析には，固定相に Amylose tris(3,5-dimethylphenylcarbamate) を含むダイセル製の CHIRALPAK IA カラム（内径 4.6 mm，長さ 25 cm，粒径 5 μm）と 2・2 に記載した機器類を使用した．カラム温度は 5 ℃ または 25 ℃ に設定し，GE の光学異性体分離を検討した．合成した GE 標準品を 2-プロパノールに 200 μg mL^{-1} の濃度になるように溶解し，その 5 μL を Rheodyne 製インジェクター（Model 7725）を用いてカラムに注入した．移動相には，アセトニトリルに少量のメタノール，2-プロパノール，エタノールまたは水（いずれも関東化学製 HPLC 用）を加えたものを使用し（組成については 3・1 参照），0.5 mL min^{-1} の流量で送液した．

2・4 キラル HPLC/APCI-MS

実試料（DAG 油）に含まれる GE の光学異性体の分離と定量にはキラル HPLC/APCI-MS を使用した．キラル HPLC は 2・3 と同一の条件で行った．APCI-MS は 2・2 と同一条件で行い，プロトン化分子を用いる選択イオン検出（SIM）により各光学異性体を定量した．合成した GE 標準品（ラセミ体）を 2-プロパノールに 0.5，1，5，10，20，50 μg mL^{-1} の濃度になるように溶解し，その 5 μL をオートインジェクター用いてカラムに注入した．溶出した各光学異性体のピーク面積を測定して検量線を作成した．検出限界と定量限界は，それぞれ $S/N = 3$，$S/N = 10$ で求めた．DAG 油は 2-プロパノールに 30 mg mL^{-1} の濃度になるように溶解し，その 20 μL をオートインジェクターを用いてカラムに注入した．移動相を 150 分間送液して，GE の後に溶出する多量の DAG などの夾雑物をカラムから排出した．

3 結果と考察

3・1 GE 標準品の純度検定

インフュージョン法による MS 分析の結果，本研究で合成したすべての GE からベースピークとして $[M+H]^+$ が検出された．また，C18 カラムを用いた逆相 HPLC/ELSD 分析では，いずれの試料からも単一のピークが得られ，合成した GE 標準品はすべて高純度であることが確認された．

3・2 キラル HPLC による GE の光学異性体分離

キラル HPLC 分析に使用した CHIRALPAK IA カラムは従来型の CHIRALPAK AD カラムと同様，固定相として Amylose tris(3,5-dimethylphenylcarbamate) を含むが，耐溶剤性に優れ，順相と逆相の両モードで使用できる特徴を有する[8]．本研究では，HPLC/MS でのイオン化を促進するために，またアシル基の異なる種々の GE の光学異性体を一斉に分離するために逆相モードを選択した．移動相にアセトニトリル/メタノール，アセトニトリル /2-プロパノール，アセトニトリル/エタノール（組成はいずれも 98.5 : 1.5, v/v），及びアセトニトリル/水（90 : 10, v/v）を用いて GE の光学異性体分離を検討した結果，アセトニトリル/メタノールで最も良い分離が得られた．たとえば，